MASTER'S THESIS

Master of Science in Advanced Mathematics and Mathematical Engineering

Title: An integrative model for perceptual decision-making and movement

Author: Alexandre Garcia-Duran Castilla

Advisors: Gemma Huguet, Alexandre Hyafil (CRM) and Manuel Molano-Mazón (CRM)

Department: Department of Mathematics

Academic year: 2022/2023

UNIVERSITAT POLITÈCNICA DE CATALUNYA
BARCELONATECH
Facultat de Matemàtiques i Estadística

Universitat Politècnica de Catalunya
Facultat de Matemàtiques i Estadística

Master in Advanced Mathematics and Mathematical Engineering

Master's thesis

An integrative model for perceptual decision-making and movement

Alexandre Garcia-Duran Castilla

Supervised by Gemma Huguet, Alexandre Hyafil, Manuel Molano-Mazón

June, 2023

First, I would like to express my sincere gratitude to my esteemed supervisors, Alexandre Hyafil and Manuel Molano, for their constant support, guidance and kindness.

I would also like to acknowledge and give special thanks to all the collaborators of the project: Jaime de la Rocha, Jordi Pastor, Lluís Hernández, Lejla Bektic, Daniel Duque and Debora Lombardo.

A special thanks to all the researchers working at the computational neuroscience labs in CRM and IDIBAPS, who also had a key role in giving advice and providing a friendly environment to work in.

Moreover, I would like to give my appreciation to my tutor Gemma Huguet, who guided and advised me in the last part of the Master's journey.

Last but not least, thanks to my family and to Elena, for their unconditional love and support.

Abstract

Acting in the natural world requires not only deciding among multiple options but also converting decisions into motor commands. The link between the dynamics of decision formation and the kinematics of response movement remains poorly understood. Here I investigate how the accumulation of decision evidence shapes response trajectories in a task where freely-moving rats combine prior expectations and acoustic information to select between two possible responses. Rats' trajectories were extracted using automatic video analysis and I found that the vigor of rats' movements is initially set by the prior expectations, and incorporates the stimulus information after the response onset by speeding their response if the stimulus supports their choice, slowing it otherwise. In trials for which the stimulus was strongly incongruent with the initial choice, rats often reversed their initial trajectories to head to the alternative port. A remarkably similar behavior was found in humans performing an analogous task under time pressure. I encapsulated this behavior in a computational model that describes the mapping between the dynamics of evidence accumulation and the full response trajectory. The model replicates the rat choices, response trajectories and explains the conditions yielding trajectory reversals. Moreover, I have found that rats' trajectories can be approximated by minimizing the jerk of their movement. Together, the results show the tight and graded relationship between the evidence accumulated during perceptual decisions and the kinematics of the response trajectories described by rats and humans to execute their choices.

Keywords

Computational neuroscience, Perceptual decision-making, Mathematical modelling, Stochastic differential equations, Optimal control theory

Contents

List of Figures

1. Introduction

Grabbing an apple at the supermarket requires not only selecting the best one, but also planning the arm's trajectory to reach it. While much progress has been made in understanding decision-making (which apple to grab) and motor control (arm trajectory to reach it given the decision), these two cognitive processes have typically been studied separately. However, in recent years, the classical view of a brain that works serially, first deciding what to do and then deciding how to do it, has been revised in favor of a perspective that describes these two processes as running in parallel [1]. This novel framework allows not only to predict motor features (the how to do it) from cognitive variables (that determine what to do), but also to leverage the study of motor kinematics to dissect the cognitive processes underlying the production of a given behavior [2]. Motor responses supporting a choice have been characterized by their speed of execution (i.e. vigor), and by the existence of changes in motor plans along their execution (i.e. trajectory updates). Vigor is positively linked to the subjective value of the chosen option [3], and tends to increase with reward, both in reaching [4] and saccadic (eye movement) [5, 6] responses. However, the effect of cognitive factors, such as the evidence towards the decision, on response vigor remains unknown. In other words, link between the dynamics of decision formation and the kinematics of response movement remains poorly understood.

On the other hand, trajectory updates have been observed when decision evidence is presented sequentially and can be incorporated into an unfolding trajectory [7, 8]. Monkeys [9, 10] and humans [11, 12] often reverse an initial choice if it is contradicted by novel sensory evidence. Yet, we do not know if this online updating of trajectories represents an isolated phenomenon that only emerges when new evidence promotes a change in the initial choice (i.e. a change of mind, CoM). Alternatively, trajectories may be routinely updated based on any novel relevant information. Discriminating between these two scenarios, as well as precisely quantifying the impact and the timing of this update, would provide invaluable information about the neural mechanisms involved in a perceptual decision, from sensory processing to the execution of a response trajectory.

To analyze vigor and trajectory updates, I investigated how response trajectories are formed as rats (n=15) integrate decision evidence in a perceptual task where decisions are guided both by an acoustic stimulus and the recent trial history [13] (Fig. 1.1). On each trial, following a 300-ms fixation period, a stimulus was played from two lateral speakers until the animal poked out from the center port and headed towards one of two side ports. Rats were rewarded if they selected the port associated with the louder speaker. The time it took for the rat to leave the port is called Reaction Time (RT). The time it took for the rat to reach the lateral port from the central one is called Movement Time (MT). The stimulus strength was manipulated parametrically. Trials were organized into repeating and alternating contexts, in which the probability to repeat the previous rewarded port was 0.8 and 0.2, respectively (Fig. 1.1 bottom). Rats leveraged this block structure and built an expectation of the next rewarded port, that we call the history-based prior [13]. This way, rats had also information about the context of each trial, and could combine it with the stimulus evidence in order to make a decision.

This prior expectation can be recapitulated by using a Generalized Linear Model of choices which quantifies the weight of different elements of recent history on choices [13, 14, 15, 16, 17]. In rats, I used the same logistic regression model as in [18] - see the reference for full model description. I defined the prior evidence as the subjective measure of how much the recent history of trials biased the current choices.

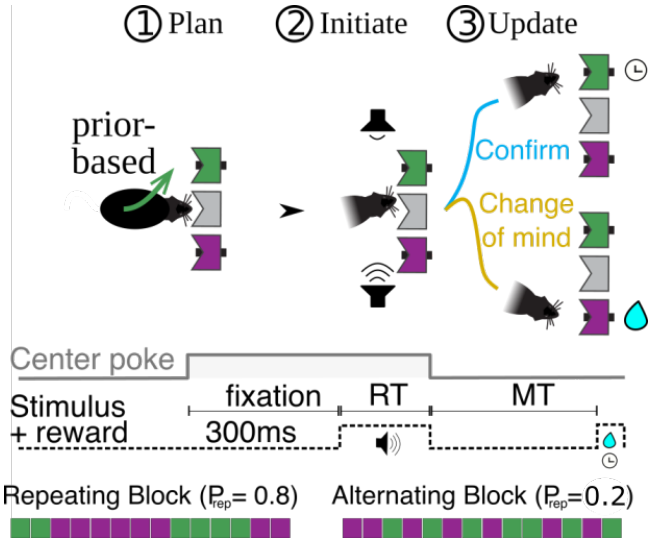

Figure 1.1: The rats' task.

On the other hand, rats' snout coordinates in the horizontal (x-y) plane were extracted from videos of the rats doing the task. To do so, we used DeepLabCut [19], a tool for automatic object tracking from videos. These trajectories have the shape shown in Fig. 1.2, whose projections along the y-axis revealed relatively stereotyped movements consisting in smooth sigmoidal-like curves starting at the central port and ending at one of the side ports. I am mostly interested in the y-dimension, since it differentiates between the right and left ports located at -80, 80 pixels, respectively.

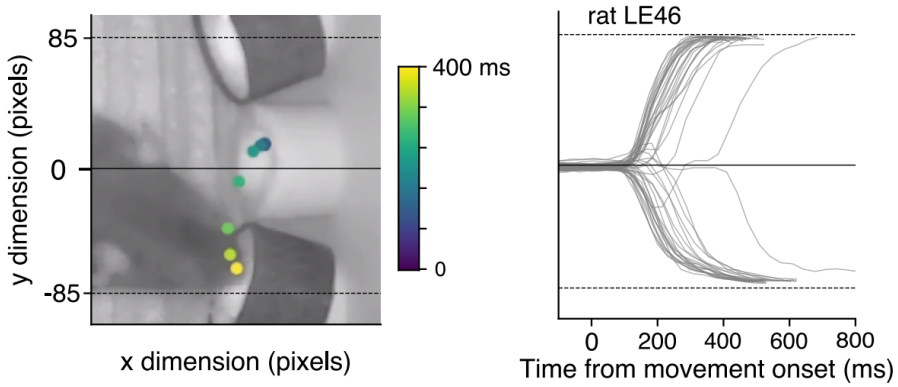

Figure 1.2: Trajectory extraction. Left: Rat's snout being tracked in the x-y plane. Points are samples taken at a constant frame rate. Right: Evolution in time of some example raw trajectories (in the y-dimension). All is done for a single rat (Rat LE46).

At this point, I have the necessary data to examine how cognitive factors, such as evidence towards the decision, affect the movements and the vigor of the animal. Moreover, I could analyze the movements of the rat and extract how trajectories are updated. This way, I could see whether decision-making and movement are serial processes or act in parallel, and try to find a link between the dynamics of decision formation and the kinematics of the motor response. In order to understand this complex process, a common approach in neuroscience is to simplify it by developing a theoretical model. This provides a framework that, given data, facilitates understanding of how changes within the framework can affect outcomes. Modelling combined

with data can explain past behavior, predict and forecast future behavior, and evaluate how changes may alter these predictions [20]. First, though, I need to understand what are the mechanisms that explain the rat behavior and movements, so I performed data analysis prior to modelling. To investigate the behavior of rats, I have the following behavioral data:

- Choice: -1 if right and 1 if left.
- Reaction Time (RT): the time it took for the rat to leave the central port since the stimulus onset.
- Movement Time (MT): the time it took for the rat to reach the lateral port from the central one.
- Evolution in time of trajectories in the $x - y$ plane.

And the experimental conditions:

- Stimulus strength: defined as the average difference in the strength of the stimulus between both sides. It takes values of 0, 0.25, 0.5, 1 (from hardest to easiest); signed by the direction of the stimulus (left or right).
- Prior evidence: real valued, going from -1 (maximum prior evidence to the right) to 1 (maximum prior evidence to the left).
- Trial index: index showing how many trials in a row has the rat been doing. It increases from 1 to the end of the session (it is variable, roughly 600 trials per session).

The data comes from Jaime de la Rocha's group in the Brain Circuits and Behavior laboratory of Institut d'Investigacions August Pí i Sunyer (IDIBAPS), extracted by Lejla Bektic, Daniel Duque and Jordi Pastor-Ciurana. The trajectories were extracted and pre-analyzed by Jordi Pastor-Ciurana, member of the laboratory.

2. Experimental results

To understand the behavior and movements of rats, I performed analysis on the data, shown in this section. It is separated in two parts, the behavioral (choice, reaction time, movement time) and the trajectory analysis.

2.1 Behavioral

In this part, I encapsulate the analysis of the behavior of rats, which encompasses the decision-making (choice) and the responding timings (RT and MT).

2.1.1 Choice

The first analysis that I did is the computation of the probability of choosing right given a stimulus and a prior evidence. To do so, I computed the proportion of rightward responses conditioning to both stimulus and prior (averaged across all rats). As seen in Fig. 2.1, rats exploit both sources of information. If both evidences are pointing to the Right, we can see that the probability of going right is maximum, whereas if they point to the left, the probability is minimum. This allow us to say that rats understand the task and exploit both sources of information to obtain the highest reward possible. To do so, they use the information from previous trials to infer the new response, and then combine it with the stimulus.

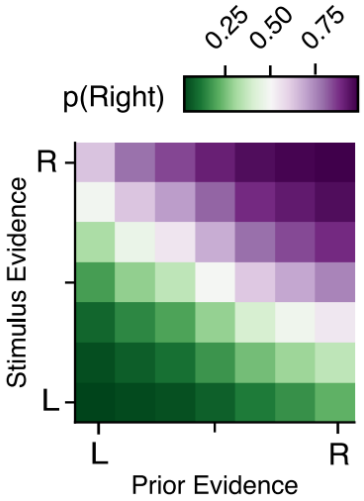

Figure 2.1: Probability of right conditioned to Stimulus and Prior evidence.

2.1.2 Reaction Time

In our experimental paradigm, the initiation of rat responses was often driven by a proactive process (rats left the central port independently on the stimulus), leading to a large fraction of reaction times that were too short to be triggered by the stimulus (known as express responses, when RT$<$ 50 ms); as seen in the density of RT conditioned on stimulus strength (Fig. 2.2 top) [21], where the distribution of RT is independent on this magnitude until RT $\sim$ 50 ms. Recall that the stimulus needs to arrive to the brain

and then be processed, then a motor action is planned and finally executed. This chain of events impose a natural latency that makes impossible for rats in these trials to process and use the stimulus before leaving the port. Despite this independence of the response onset on the stimulus, the final choice made by the rat integrated the stimulus evidence: its accuracy increased with stimulus strength easiness, as seen in the so known tachometric curves (Fig. 2.2 bottom), which represent the accuracy depending on the RT and conditioned to stimulus strength. That would mean that the stimulus has been processed somewhere between leaving the central port (at this point the stimulus is off) and reaching the response port. This implies that in a large fraction of trials, rats process the stimulus and update their decision en route, somewhere between the central port and the lateral port. I therefore set out to look for signatures of the decision making variables on the rats' response trajectories.

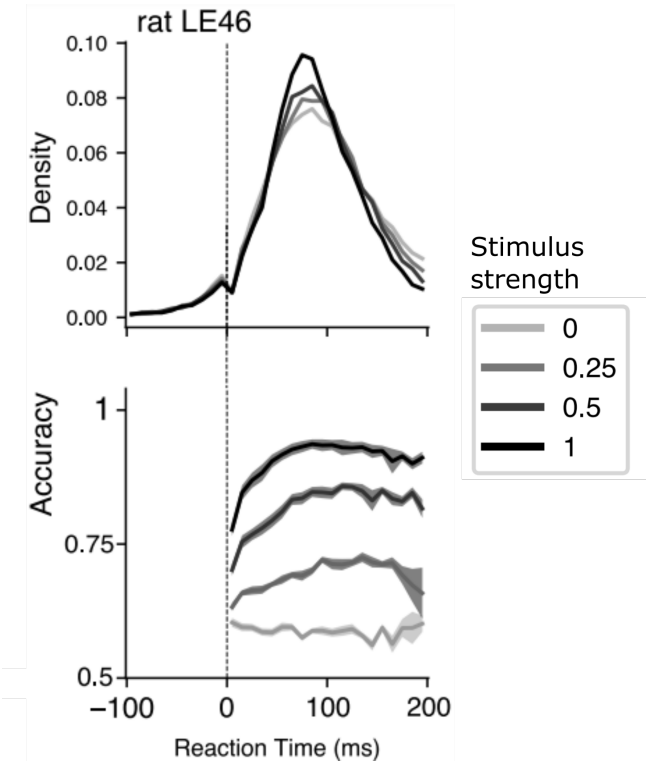

Figure 2.2: Top: Reaction time distribution conditioned at stimulus evidence. Bottom: Evolution of accuracy conditioned to stimulus strength w.r.t. RT (tachometric curve). All for the same rat LE46.

2.1.3 Movement Time

Then I analyzed the Movement Time (MT), which is related to vigor (inversely proportional). I analyzed the MT conditioned to both prior and stimulus evidence. Firstly, I defined the prior congruency (with the final response) as how much prior the rat has towards the choice done, and are positive (congruent) when pointing at the same direction and negative (incongruent) otherwise. I found that the stronger the prior towards the selected port was, the shorter the movement time was (Fig. 2.3). In contrast, when the prior evidence pointed against the selected port, the animal took longer. Secondly, I analyzed the impact of stimulus evidence on the movement time, restricting our analysis to trials with small prior magnitude, and defined the stimulus evidence congruency similar as before, how much the stimulus is pointing to the final response. Recall that if this magnitude is negative, the response done is incorrect, since the stimulus carries the ground truth. I found that similarly to the impact of prior evidence, rat movement responses were faster when the stimulus supported the selected port, and slower when the stimulus was in disagreement with it (Fig. 2.4).

Remark 2.1. The legends in Figures 5 and 6 will be used along the document.

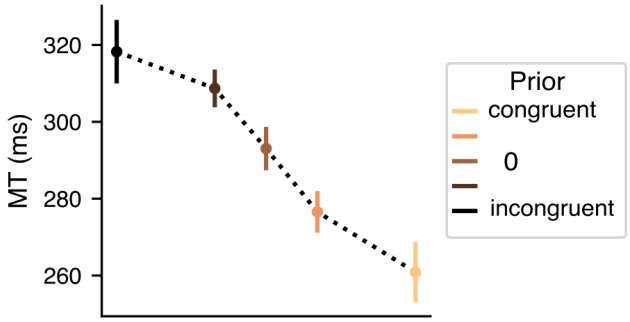

Figure 2.3: Movement time conditioned to prior congruency with the final response. Only for silent trials (i.e. with no stimulus displayed).

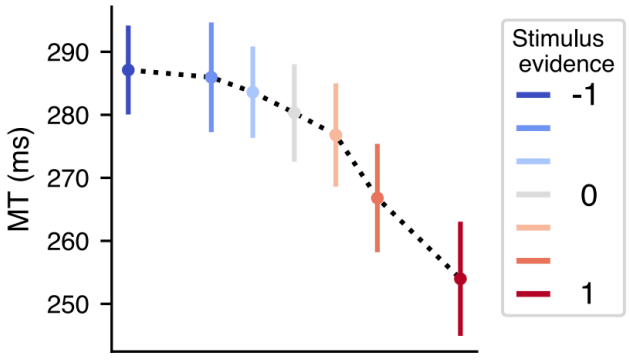

Figure 2.4: Movement time conditioned to stimulus evidence, i.e. stimulus congruency with the final response. Trials with RT$<$ 50 ms, to show that even if the stimulus cannot be integrated before leaving the center port, the stimulus still affects the movement.

When assessed altogether, MT depended on a linear combination of stimulus and prior evidence towards the response, shown in a simple linear regression of the z-scored MT, with the following expression $MT \sim stimulus, prior, trial\ index$ (Fig. 2.5). We can see that both have a significant negative weight value, showing this negative linear relationship seen before. Trial index had a positive value, but was not included in this plot for simplification. If we take a look at the relation between MT and trial index (Fig. 2.6) we can see the reason of this positive relation.

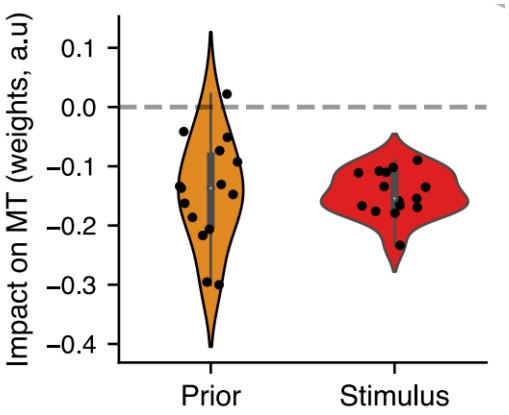

Figure 2.5: z-scored MT regression weights.

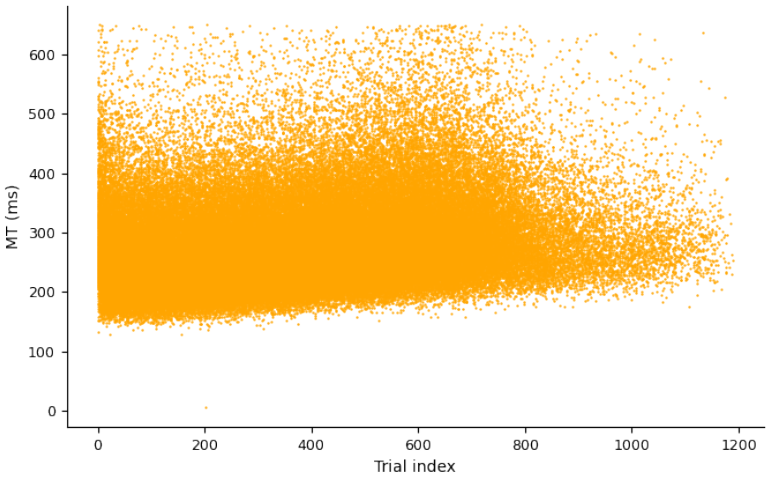

Figure 2.6: Movement Time (MT) vs trial index for a single rat (LE43).

Therefore, both prior and stimulus evidence impact the overall vigor with which rats perform the response movement.

2.2 Trajectories

The previous results suggest that prior and stimulus evidence have an impact on the overall vigor with which rats execute their decision. However, movement times cannot tell us anything about the timing

of that impact nor about the trajectories described by the rats for different decision variables. Indeed, the same movement time could correspond to very different trajectory shapes. Therefore, I analyzed the trajectories similarly as the vigor. The trajectories became steeper as the prior and stimulus evidence more strongly supported the selected port (Fig. 2.7, top left and right, respectively). Indeed, the stronger the prior towards the selected port was the higher the peak velocity of the animal movement (Fig. 2.7, bottom left). Similarly, rats reached larger velocities when the stimulus supported the selected port than when the stimulus was in disagreement with it (Fig. 2.7, bottom right). Therefore, the correlation between movement time and evidence described in the previous section is accompanied by an increase in peak velocity for more congruent decision evidence. The trajectories conditioned on prior evidence seem to diverge earlier than those conditioned on stimulus evidence (Fig. 2.7). This is consistent with the evolution of the two variables: while the prior information is available at the trial start and hence impacts the trajectories soon after the response onset, sensory evidence must be integrated as the stimulus is played. Thus, the precise timing of the stimulus impact hinges on the duration of a chain of sensorimotor processes that include afferent (sensory) delays, evidence integration, efferent (motor) and kinematic delays.

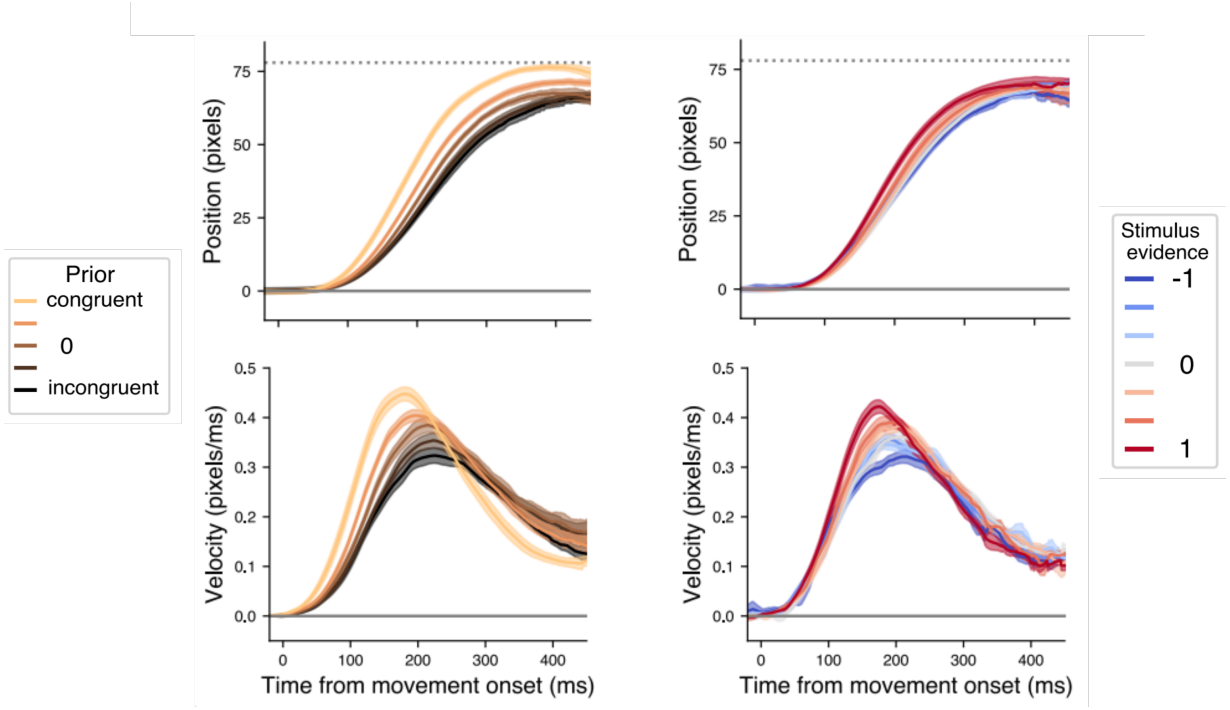

Figure 2.7: Top: rat trajectories in the y-axis. Bottom: rat velocities in the y-axis. Both magnitudes conditioned to prior congruency (left, silent trials) and stimulus evidence (right, trials with RT < 0).

2.2.1 Trajectory reversal

The above results show that trajectories are not predefined ballistic movements but they are dynamically sped up or slowed down in response to new sensory evidence. Importantly, previous studies in primates have shown that new sensory evidence can lead to changes of mind (CoMs) or trajectory reversals, i.e. a change in the response trajectory towards a different option that is aligned with the novel information [11, 22, 12, 23]. I investigated whether rats in our task also perform changes of mind.

I identified possible CoMs by selecting trials where the trajectory crossed an imaginary threshold towards one of the lateral ports but ultimately reversed and reached the opposite port. Trajectory reversals were associated with a stereotyped trajectory that shows a clear deflection from their path towards the initial choice, as shown in Fig. 2.8, where we see the average evolution in time of the rat in the y-axis, for reversals and non-reversals trajectories.

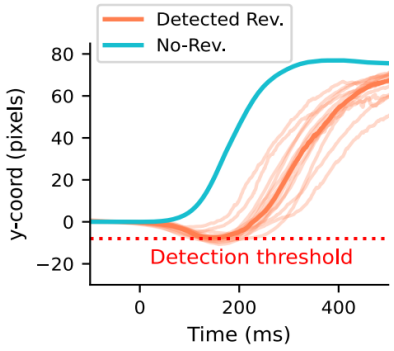

Figure 2.8: Average trajectory across rats in reversals (salmon) versus non reversal (blue).

I then tested whether these trajectory reversals corresponded to changes of mind, whereby a first decision driven by the prior evidence is later switched based on sensory evidence contradicting the prior. To do so, I calculated the probability of observing a trajectory reversal as a function of prior and stimulus evidence, separately for Left-to-Right and Right-to-Left reversals (Fig. 2.9). Crucially, trajectory reversals usually emerged when the prior and stimulus were incongruent, as the initial response is aligned with the prior while the final response is aligned with the stimulus. Therefore, since the stimulus contains the ground truth, these reversals are corrective and thus are CoMs.

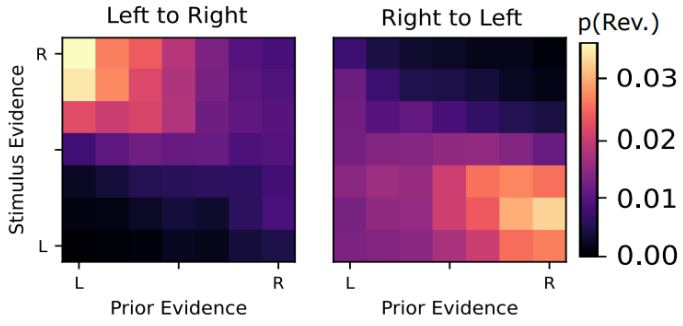

Figure 2.9: Left and Right: Probability of reversal as a function of both prior and stimulus, conditioned to Right and Left responses, respectively.

To sum up, we have seen that decision-making and motor responses act in parallel, and the sensory

integration updates the trajectory with the information that has not been still integrated while the animal is moving.

2.3 Human data

I replicated the results obtained in rats in a novel task in human participants (N=20) that mimicked the rat task (Appendix A.1, Fig. A.1). The experimental data used for the analyses was extracted by Debora Lombardo and myself. Doing the same analyses as before, I found a remarkably similar behavior between rats and humans. All human data analysis can be found in Appendix A.1. Roughly, humans exploit both sources of information (prior and stimulus, Appendix A.1, Fig. A.2), and the response trajectories were impacted by both the stimulus and the prior in a similar fashion, leading to trajectory reversals too (Appendix A.1, Fig. A.3, A.4, A.5). An important difference between the behavior observed in humans and rats is that the former performed many more trajectory reversals (Appendix A.1, Fig. A.6). Part of this difference is likely due to our greater capacity to detect reversals in the psychophysical experiment. However, it is also worth noting that in the psychophysical experiments, where humans just have to respond by moving the arm or finger, the cost of a change of mind is much smaller than in a full-body task like the rats experiments and therefore, subjects might be more prone to change their mind. In the future it will be important to elucidate under which circumstances the similarities observed in our task between humans and rats breaks.

This similarity between rats and humans suggests that the strategies used by the two species to process asynchronous information evolved before the two species diverged around 75 million years ago [24]. It would also suggest that these same mechanisms control the link between very different motor movements, such as the full-body displacement done by the rats or the sliding of the finger performed by the human subjects. Consistent with this hypothesis, the basal ganglia, which has been implicated with the control of vigor [25], evolved with the emergence of the first vertebrates 500 million years ago [26] and has been conserved since then. This conservation may reflect the fact that the type of embodied decisions explored in this work, in which the subject acts while deciding and decides while acting [27], have been fundamental throughout the evolutionary history of vertebrates.

3. Modelling rats' behavior

In this section, I will explain the modelling of the behavior and movements of the rat in the decision-making task shown in the previous section. Roughly, my scope is to develop a model that replicates the rat responses and trajectories, receiving as input only the experimental conditions, i.e. prior evidence, stimulus evidence and trial index. To do so, we will need a model able to integrate a stimulus and produce a trajectory, with the possibility of an update *en route*, due to the incoming of new sensory evidence. I have separated the modelling in two main stages, the sensory integration and the trajectory generation, acting in parallel, with a bridge to link both since we have seen this tight and graded connection in the experimental data.

3.1 Modelling the sensory integration

For this part, I used an evidence accumulation model (EAM), which is a class of computational cognitive model used to understand the latent cognitive processes that underlie animal decisions and reaction times (RT) [28]. To be more specific, I used the Drift-Diffusion Model (DDM) [29], explained below.

3.1.1 Drift-Diffusion Model (DDM)

The DDM summarizes the evidence supporting the different options into a decision variable that evolves in time until it reaches a bound that determines the choice. This intuitive paradigm generates precise predictions about how choices and reaction times depend on stimulus evidence [30, 31, 32, 33], as well as on key behavioral variables such as prior expectations [34, 35, 29]. This model is based on a stochastic process defined by a stochastic dynamical equation that represent a linear noisy integration in time, which denotes the Evidence Accumulation (EA). The mentioned equation is

$$X_t = \nu\ t + \sigma\ W_t\ , \tag{1}$$

where X_t is called the decision variable, ν is the integration drift and W_t is a standard Wiener process, which will produce the diffusion. The subindex $(\cdot)_t$ represents the time index t. Therefore, it evolves in time by the addition of two terms, a drift (related to stimulus) and a noise (related to internal noise, responsible of diffusion).

Definition 3.1. (Stochastic process) Suppose that $(\Omega, \mathcal{F}, \mathbb{P})$ is a probability space, and that $I \subset \mathbb{R}$ is of finite cardinality. Suppose further that for each $\alpha \in I$, there is a random variable $X_\alpha : \Omega \to \mathbb{R}$ defined on $(\Omega, \mathcal{F}, \mathbb{P})$. The function $X : I \times \Omega \to \mathbb{R}$ defined by $X(\alpha, w) = X_\alpha(w)$ is called a *stochastic process* with indexing set I, and is written $X = \{X_\alpha, \alpha \in I\}$

Definition 3.2. (Brownian motion or Wiener process) A standard (one-dimensional) Brownian motion is a stochastic process $\{W_t\}_{t\geq 0}$ indexed by non-negative real numbers t, defined on a probability space $(\Omega, \mathcal{F}, \mathbb{P})$, with the following properties:

1. $W_0 = 0$.
2. With probability 1, the function $t \to W_t$ is continuous in t.
3. The process $\{W_t\}_{t\geq 0}$ has stationary, independent increments.

4. The increment $W_{t+dt} - W_t$ has the Normal $\mathcal{N}(0, \sigma^2 dt)$ distribution, for all $dt, t \geq 0, \sigma^2 > 0$.

A $d-$dimensional Wiener process is a vector-valued stochastic process

$$W_t = \left(W_t^{(1)}, W_t^{(2)}, \dots, W_t^{(d)}\right) .$$

Definition 3.3. (Standard Wiener process) The Standard Wiener process is a Wiener process with $\sigma = 1$.

Regarding the initial condition, is common to assume that $X_{t=0} = 0$. For the decision-making framework, the stimulus s is encoded in ν, as $\nu = s \cdot p_s$, where p_s is the weight given to the stimulus, a free parameter of the model. Moreover, there are two bounds $(a_e, -a_e)$ that represent the limits of the integration. Indeed, if $X_t = a_e, -a_e$ the decision is made, reactively to the stimulus, to one choice or the other (characterized by the bounds). In addition, the first time that $|X_t| \geq a_e$ is called first-time passage, or Reaction Time (RT). In our case, a_e and $-a_e$ could represent left and right responses, respectively, and are free parameters of the model. For our initial condition, since we have a quantification of the context expected by the rat z, we can implement it with a bias term Z such that the initial conditions are modified as $X_{t=0} = Z$, and $Z = z\ p_z$, where p_z is the weight of the prior evidence, a free parameter. For convenience, we set $\sigma = 1$. Given that we do a discrete integration, we can express the model as

$$X[n] = X[n-1] + \nu\ dt + \sigma\ W[n]\ \sqrt{dt} \quad \text{for } n = 1, 2, 3, \dots$$

where n is the discrete index, and dt is the timestep, which is 5 ms, and $X[0] = Z$. The square root of dt comes from the third property of the standard Wiener process, where Wiener process increment follows a Normal distribution with variance dt, $W_{t+dt} - W_t \sim \mathcal{N}(0, dt) = \sqrt{dt}\mathcal{N}(0, 1)$. Therefore, $W[n]$ is a random variable sampled from a normal distribution of mean 0 and variance 1.

Regarding the timings of integration, I impose a delay in the integration due to natural constraints for the stimulus to reach the brain, which is called afferent time, t_{aff}, and is a free parameter of the model. Then, when the decision variable reaches the bound, there is a motor delay also, to represent the time it takes for the brain to send and execute the motor order, and is called efferent time, t_{eff}; which is also a free parameter. In Fig. 3.1, we can see a schematic of the model. The integration starts with some bias term (Z) and no drift $(\nu = 0$, since there is no stimulus in yet, i.e. $s = 0)$, and when the stimulus arrive, the integration has to wait for the afferent time $(t_{aff}$, time for the stimulus to reach the processing zone in the brain), then the stimulus impacts the integration with a drift (ν) towards one of the bounds a_e. Then, when the decision variable reaches the bound, the reaction time is computed as the total time since the stimulus onset until the reaching plus the efferent time t_{eff}, which is the time needed to send a motor order and perform the movement.
As a simple extension, we can add leak, which is parameterized by λ, and expresses the proportion of information that is forgotten between two sequential steps, so we have

$$X[n] = X[n-1]\ (1 - \lambda) + \nu\ dt + \sigma\ W[n]\ \sqrt{dt}$$

To sum up, we have a model that integrates a stimulus with leak, which considers natural latencies and a context, or prior evidence, and gives values of choice and reaction time.

3.1.2 Extended DDM

The responses given by the previous model are reactive, since they are triggered in reaction to stimulus presentation when the accumulated stimulus evidence reaches a decision threshold. However, this framework

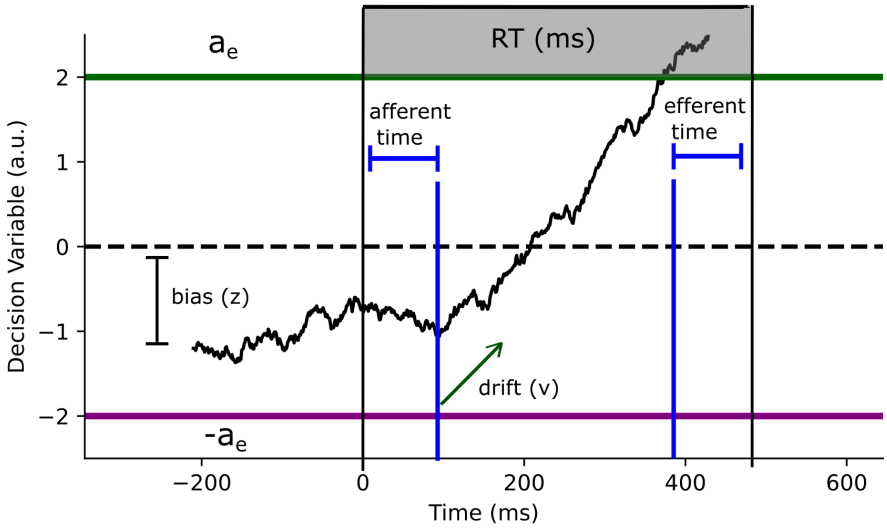

Figure 3.1: Standard DDM schematic.

excludes the possibility that informed responses are generated proactively at a time independent of stimulus, which has been seen in rats (Fig. 2.2). To model this part, I added an independent Action Initiation (AI) process which reflects the preparation of a response, as done by Hernández-Navarro et al. [21]. This process is similar as the one before

$$A_t = \nu_A \; t + \sigma \; W_t \; ,$$

where A_t is the value of Action and v_A the drift of the Action. The other magnitudes represent the same as before. There is one single bound (called Go bound), a_A, another free parameter of the model. Similar as before, there is a time latency t_A that must pass before the action can start integrating, a free parameter. Finally, the total reaction times arise from the competition between both processes: if the AI process hits the Go bound first (proactive response) a response is triggered, and the choice is given by the sign of the accumulated evidence at that moment. This procedure is equivalent to an instantaneous collapse of Evidence Accumulation (EA) bounds. In proactive responses, the timing of the response is thus completely independent of the stimulus strength. Conversely, if EA reaches a decision bound first (reactive response), it sets both RT and choice, and AI plays no role, as in a standard DDM.
In this case, the Action drift ν_A will depend negatively on the trial index TI, reflecting the tiredness of the animal (the longer the session, the greater the reaction times), such that $\nu_A = p_{A,0} - p_{A,1} \cdot \text{TI}$, where $p_{A,0}, p_{A,1} > 0$ are the intercept and the slope, respectively, of the linear relationship of the action drift with the trial index and are free parameters of the model.

3.1.3 Workflow of the model

A schematic of this process is shown in Fig. 3.2. The two processes start at t =-300 ms. $X_{-300} = Z$ and $A_{-300} = 0$. In order to get positive time indexes, we could just define the time from the fixation onset, so $\hat{t} = t + 300$ ms, but for simplification I will maintain the negative time notation. First, the action starts integrating after an offset time t_A, with a drift V_A (Fig.3.2 bottom). When $t = 0$, the stimulus appears (stimulus onset) and arrives after some time t_{aff} in the evidence accumulator process so it can begin to

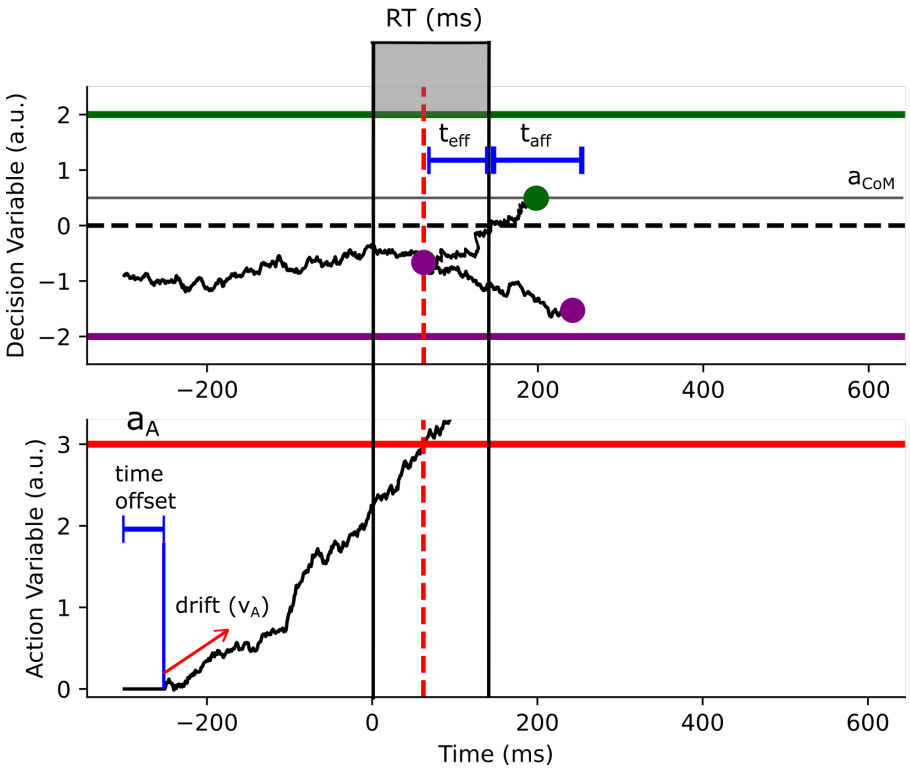

Figure 3.2: Extended DDM schematic.

integrate with drift ν (Fig.3.2 top). The first of the two processes that reaches a respective bound (called the first read-out, first purple dot in Fig.3.2 top, since the evidence points to the right response), will fire the response of the animal, which will be executed after an efferent delay t_{eff}. Therefore, the RT is defined as the time of the first reaching plus the efferent delay. In this case, the Action has triggered the response, which is a proactive one. Then, all the information from the stimulus that has not arrived yet to the brain due to the latency t_{aff}, can still be integrated as decision variable, and a second read-out is performed after this time (second purple dot in Fig.3.2 top, since the evidence points to the right response). In order to enable the model to produce Changes of Mind (CoM), we can define a bound, a_{CoM}, which if is reached by the decision variable at the second read-out stage, the response will change, green dot Fig.3.2 top, since the CoM bound is reached and thus the decision is changed.

Remark 3.4. We define t_{updt} as the time between the first and second read-out. In non-reversal trials, $t_{updt} = t_{eff} + t_{aff}$, and for reversals, is the time it takes to reach the CoM bound.

To sum up, we have a sensory integrator model that performs decisions and possible updates, with the possibility of a change of mind. With this, we have values of RT, choice and decision variable for reach moment in time.

3.2 Modelling the trajectory

Our objective in this section will be to model the trajectory of the rat. This way, we would have a complete model which integrates stimulus evidence given certain prior conditions and expresses the trajectory of

the animal. In order to model it, we must consider trajectories satisfying certain optimal characteristics that reflect naturalistic movements and constraints. To explore and compute them, I used optimal control theory. Optimal control tries to find input functions $u(t)$, $u \in \mathbb{R}^d$, and the corresponding state trajectories $x(t)$, $x \in \mathbb{R}^d$, that maximize performance (or minimize a cost) under constraints [36, 37, 38]. An example of optimal control problem (OCP) is given below:

$$\min_{x(t),u(t)} \quad \mathcal{S}(u(t), x(t))$$

$$\begin{gathered} \text{subject to } \dot{x}(t) = f(x(t), u(t)) \\ x(0) = \hat{x}_0 \\ x(T) = \hat{x}_T \\ u_{min} \leq u(t) \leq u_{max} \\ x_{min} \leq x(t) \leq x_{max} \end{gathered}$$

where $\mathcal{S}$ is the functional, which represents action (i.e. cost), a scalar quantity describing how a physical system has changed over time. It takes a d-dimensional input and returns an scalar, $\mathcal{S} : \mathbb{R}^d \to \mathbb{R}$. It is the quantity that we want to minimize, so in the end we are minimizing the cost. The dynamical equation $\dot{x}(t) = f(x(t), u(t))$ enforces the dynamics of the system, $\hat{x}_0$ and $\hat{x}_T$ are the given initial and final states, and $u_{min}, u_{max}, x_{min}, x_{max}$ are some boundary conditions. To sum up, the solution of this problem is the one that minimizes (or extremizes) the functional $\mathcal{S}$ given some constraints. Now, we have to define the functional to minimize, which depends on what we want to minimize. We could minimize, for example:

- $\dot{x}(t)$, velocity, and we would obtain the shortest path.
- $\ddot{x}(t)$, acceleration.
- $x^{(3)}(t)$, jerk.
- $x^{(4)}(t)$, span.

We would like to generalize the procedure, so we define $x^{(r)}$ as the r derivative of the position x with respect to the time t. The functional will be the integral of a quantity, called the Lagrangian $\mathcal{L}$, which can depend on t, $x(t)$ and any time-derivative of x, such as

$$\mathcal{S}(x(t)) = \int_{t_i}^{t_f} \mathcal{L}(t, x(t), \dot{x}(t), \ddot{x}(t), \dots, x^{(r)}(t))\, dt\,. \tag{2}$$

In order to minimize it, I used the theorem 3.6. The theorem is for $r = 1$.

Definition 3.5. Let $\mathcal{C}^k[a, b]$ denote the set of continuous functions defined on the interval $a \leq x \leq b$ which have their first k-derivatives also continuous on $a \leq x \leq b$.

Theorem 3.6. *Let $I(Y)$ be an extremum of the functional*

$$I(y) = \int_a^b F(x, y(x), y'(x))dx$$

defined on all functions $y \in \mathcal{C}^2[a, b]$ such that $y(a) = A$, $y(b) = B$, and F a $\mathcal{C}^2$ function, then $Y(x)$ satisfies the second order differential equation

$$\frac{d}{dx}\frac{\partial F}{\partial y'} - \frac{\partial F}{\partial x} = 0\,. \tag{3}$$

Definition 3.7. Equation (3) is the Euler-Lagrange equation, or sometimes just Euler's equation.

3.2.1 Derivation of the Euler-Lagrange equation

Assume that the function $x \in \mathcal{C}^2[a,b]$ which satisfies the boundary conditions $x(a) = A$, $x(b) = B$, extremizes the functional

$$\mathcal{S}(x) = \int_a^b \mathcal{L}(t, x(t), \dot{x}(t))\, dt\ .$$

We assume that $\mathcal{L}$ is at least $\mathcal{C}^2$. Now we want to consider an infinitesimally small variation of x, δx. For this we define the variation as $\delta x := \varepsilon\eta$, and the perturbed trajectory will be $x_\varepsilon(t) = x(t) + \varepsilon\eta(t)$. Here ε is a very small real number and $\eta(t)$ is an arbitrary differentiable function defined in the interval $[a,b]$ such that $\eta(a) = \eta(b) = 0$. In other words: the perturbed trajectory must pass through the boundary points. Let us define the variation of the functional,

$$\mathcal{S}(x_\varepsilon) = \int_a^b \mathcal{L}(t, x_\varepsilon(t), \dot{x}_\varepsilon(t))\, dt\ . \tag{4}$$

Let us expand the Lagrangian function around the point $\varepsilon = 0$ up to 1st order (where I have dropped the dependence on t and abbreviated $\mathcal{L}(t, x_\varepsilon(t), \dot{x}_\varepsilon(t)) := \mathcal{L}_\varepsilon$ and $\mathcal{L}(t, x(t), \dot{x}(t)) := \mathcal{L}$ to ease the notation)

$$\mathcal{L}_\varepsilon = \mathcal{L} + \varepsilon \left(\left.\frac{\partial \mathcal{L}_\varepsilon}{\partial \varepsilon}\right|_{\varepsilon=0} \right) + \mathcal{O}(\varepsilon^2)\ . \tag{5}$$

Next, we need to compute the derivative of $\mathcal{L}_\varepsilon$ with respect to ε and evaluate it at $\varepsilon = 0$

$$\left.\frac{\partial \mathcal{L}_\varepsilon}{\partial \varepsilon}\right|_{\varepsilon=0} = \frac{\partial \mathcal{L}}{\partial x}\eta + \frac{\partial \mathcal{L}}{\partial \dot{x}}\dot{\eta}\ .$$

Then, we can plug in Eq. (4) the full expression of the expanded Lagrangian (5),

$$\mathcal{S}(x_\varepsilon) = \int_a^b \left(\mathcal{L} + \varepsilon\frac{\partial \mathcal{L}}{\partial x}\eta + \varepsilon\frac{\partial \mathcal{L}}{\partial \dot{x}}\dot{\eta} + \mathcal{O}(\varepsilon^2) \right)\, dt = \mathcal{S}(x) + \int_a^b \left(\varepsilon\frac{\partial \mathcal{L}}{\partial x}\eta + \varepsilon\frac{\partial \mathcal{L}}{\partial \dot{x}}\dot{\eta} + \mathcal{O}(\varepsilon^2) \right)\, dt\ .$$

Now, we see that

$$\mathcal{S}(x_\varepsilon) - \mathcal{S}(x) = \varepsilon \left[\int_a^b \left(\frac{\partial \mathcal{L}}{\partial x}\eta + \varepsilon\frac{\partial \mathcal{L}}{\partial \dot{x}}\dot{\eta} \right)\, dt \right] + \mathcal{O}(\varepsilon^2)\ .$$

The term in brackets is called the first variation of the action, and it is denoted by the symbol $\delta\mathcal{S}$.

$$\delta\mathcal{S} = \int_a^b \left(\frac{\partial \mathcal{L}}{\partial x}\eta + \varepsilon\frac{\partial \mathcal{L}}{\partial \dot{x}}\dot{\eta} \right)\, dt\ .$$

For $\mathcal{S}$ to be stationary, the first variation of the action must be zero, i.e. $\delta\mathcal{S} = 0$, for any small arbitrary variation δx (i.e. any arbitrary small ε). Therefore, we have that

$$\int_a^b \frac{\partial \mathcal{L}}{\partial x}\eta + \frac{\partial \mathcal{L}}{\partial \dot{x}}\dot{\eta}\ dt = 0\ . \tag{6}$$

The integral will be computed separately regarding the added terms. First, integrating by parts the second term,

$$\int_a^b \dot{\eta}(t)\ \frac{\partial \mathcal{L}}{\partial \dot{x}} dt = \left[\eta(t)\ \frac{\partial \mathcal{L}}{\partial \dot{x}} \right]_a^b - \int_a^b \eta(t) \frac{d}{dt}\left(\frac{\partial \mathcal{L}}{\partial \dot{x}} \right)\, dt$$

since $\eta(a) = \eta(b) = 0$,

$$\int_a^b \dot{\eta}(t)\frac{\partial \mathcal{L}}{\partial \dot{x}} dt = -\int_a^b \eta(t)\frac{d}{dt}\left(\frac{\partial \mathcal{L}}{\partial \dot{x}}\right) dt \ ,$$

and if we combine it with Eq. (6),

$$\int_a^b \eta(t)\frac{\partial \mathcal{L}}{\partial x} - \eta(t)\frac{d}{dt}\left(\frac{\partial \mathcal{L}}{\partial \dot{x}}\right) dt = \int_a^b \eta(t)\left[\frac{\partial \mathcal{L}}{\partial x} - \frac{d}{dt}\left(\frac{\partial \mathcal{L}}{\partial \dot{x}}\right)\right] dt = 0 \ . \tag{7}$$

Here we use the Fundamental Lemma of the Calculus of Variations (FLCV).

Lemma 3.8. *(FLCV) Let $y(x)$ be continuous on $[a, b]$, and suppose that for all $\eta(x) \in \mathcal{C}^2\ [a, b]$ such that $\eta(a) = \eta(b) = 0$ we have*

$$\int_a^b y(x)\eta(x)\ dx = 0 \ .$$

Then, $y(x) = 0$ for all $a \leq x \leq b$.

Since $\eta \in \mathcal{C}^2\ [a, b]$ is an arbitrary function satisfying $\eta(a) = \eta(b) = 0$ and the expression multiplying $\eta(t)$ is continuous in $[a, b]$, using Lemma 3.8 in Eq. (7) we have

$$\frac{\partial \mathcal{L}}{\partial x} - \frac{d}{dt}\left(\frac{\partial \mathcal{L}}{\partial \dot{x}}\right) = 0 \tag{8}$$

which is the Euler-Lagrange equation.

3.2.2 The rats' trajectory

Given that the examples shown before represent up to r derivatives of the position x w.r.t. time t, there is a generalized Euler-Lagrange equation for r derivatives [39], which is

$$\frac{\partial \mathcal{L}}{\partial x} + \sum_{k=1}^{r}(-1)^k \frac{d^k}{dt^k}\left(\frac{\partial \mathcal{L}}{\partial x^{(k)}}\right) = 0 \ . \tag{9}$$

Derivation. We consider the following functional

$$\mathcal{S}(x) = \int_a^b \mathcal{L}(t, x(t), \dot{x}(t), \ddot{x}(t), \dots, x^{(r)}(t))\ dt \ .$$

Again we take $\eta(t)$ to be an arbitrary function at least $\mathcal{C}^{2r}[a, b]$, and vanishing at the boundaries, such that $\eta(t) = \dot{\eta}(t) = \ddot{\eta} = \cdots = \eta^{(r-1)}(t) = 0$ when $t = a, b$. Just as before we obtain for the first variation of the action $\delta\mathcal{S}$

$$\delta\mathcal{S} = \int_a^b \left(\frac{\partial \mathcal{L}}{\partial x}\eta(t) + \frac{\partial \mathcal{L}}{\partial \dot{x}}\dot{\eta}(t) + \cdots + \frac{\partial \mathcal{L}}{\partial x^{(r)}}\eta^{(r)}(t)\right)\ dt = 0 \ .$$

By repeated integration by parts we can eliminate all the derivatives of the function η from the integral, transforming it into the form

$$\int_a^b \eta(t)\frac{\partial \mathcal{L}}{\partial x} - \eta(t)\frac{d}{dt}\left(\frac{\partial \mathcal{L}}{\partial \dot{x}}\right) + \eta(t)\frac{d^2}{dt^2}\left(\frac{\partial \mathcal{L}}{\partial \ddot{x}}\right) - \cdots + (-1)^r\eta(t)\frac{d^r}{dt^r}\left(\frac{\partial \mathcal{L}}{\partial x^{(r)}}\right) dt = 0.$$

Thus, by the fundamental lemma 3.8, we obtain the differential equation of order $2r$

$$\frac{\partial \mathcal{L}}{\partial x} - \frac{d}{dt}\left(\frac{\partial \mathcal{L}}{\partial \dot{x}}\right) + \frac{d^2}{dt^2}\left(\frac{\partial \mathcal{L}}{\partial \ddot{x}}\right) - \cdots + (-1)^r \frac{d^r}{dt^r}\left(\frac{\partial \mathcal{L}}{\partial x^{(r)}}\right) = \frac{\partial \mathcal{L}}{\partial x} + \sum_{k=1}^{r} (-1)^k \frac{d^k}{dt^k}\left(\frac{\partial \mathcal{L}}{\partial x^{(k)}}\right) = 0\,,$$

which is the generalization of the Euler-Lagrange for a single function of single variable with higher derivatives (Eq. (9)).

Now we have to choose the quantity that we want to minimize. For a decision-making task in humans where they have to move the hand to respond, it has been shown that, with learning and practice, movements tend to be performed more smoothly and gracefully, which may indicate an underlying objective of achieving the smoothest movement which carries the hand from one equilibrium position to another [40, 41]. On the other side, it has been shown smoothness can be quantified as a function of jerk [42, 43, 44], which is the time derivative of acceleration. Moreover, previous studies found that for a system to move smoothly from one point to another, it should minimize the sum of the squared jerk along its trajectory [3, 45, 46, 47]. Hence, to satisfy this condition, the Lagrangian becomes

$$\mathcal{L}(t, x^{(3)}(t)) = ||x^{(3)}(t)||^2\,. \tag{10}$$

In line with the literature, we will use the minimum-jerk trajectory ($r = 3$). So Eq. (9) for $r = 3$ becomes

$$\frac{\partial \mathcal{L}}{\partial x} - \frac{d}{dt}\left(\frac{\partial \mathcal{L}}{\partial \dot{x}}\right) + \frac{d^2}{dt^2}\left(\frac{\partial \mathcal{L}}{\partial \ddot{x}}\right) - \frac{d^3}{dt^3}\left(\frac{\partial \mathcal{L}}{\partial x^{(3)}}\right) = 0\,.$$

And since $\mathcal{L} = ||x^{(3)}\,(t)||^2$, it only depends on $x^{(3)}$. Therefore, the equation gets reduced to

$$\frac{d^3}{dt^3}\left(\frac{\partial \mathcal{L}}{\partial x^{(3)}}\right) = 0 \implies \frac{d^3}{dt^3}(2||x^{(3)}(t)||) = 0 \implies x^{(6)}(t) = 0 \tag{11}$$

since all the other derivatives banish. Given the structure of the Lagrangian, we could generalize it for any value of r, i.e. $\mathcal{L}(t, x^{(r)}(t)) = ||x^{(r)}(t)||^2$. Then, the solutions for other magnitudes minimized have a fixed composition regarding the value of r:

- Acceleration minimization: $x^{(4)}(t) = 0$.
- Span minimization: $x^{(8)}(t) = 0$.

since the Euler-Lagrange equation for any r (Eq. (9)) will end up being

$$\frac{d^r}{dt^r}\left(\frac{\partial \mathcal{L}}{\partial x^{(r)}}\right) = 0.$$

Therefore, for this type of Lagrangian, if the quantity to minimize is $x^{(r)}$, the equation satisfying this extrema will be

$$x^{(2r)}(t) = 0\,. \tag{12}$$

There are alternative ways to derive the solution in Eq. (11), shown in the following section.

3.2.3 Alternative derivation of the solution

As before, we should minimize the following functional $\mathcal{S}(x(t))$, which can be interpreted as the jerk cost.

$$\mathcal{S}(x(t)) = \int_{t_i}^{t_f} ||x^{(3)}(t)||^2 dt = \int_{t_i}^{t_f} \mathcal{L}(t, x^{(3)}(t)) dt$$

Where t_i and t_f are the initial and final times of the trajectory. Therefore, we want $x^*(t)$, solution of $x^*(t) = \arg\min_{x(t)} \mathcal{S}(x(t))$. If $\mathcal{S}(x(t))$ attains a local minimum at $x^*(t)$, and $\eta(t)$ is an arbitrary function that has at least one derivative and vanishes at the endpoints of the trajectory $x(t_i), x(t_f)$, therefore $\eta(t_i) = \eta(t_f) = 0$, then for any ε close to zero,

$$\mathcal{S}(x^*(t)) \leq \mathcal{S}(x^*(t) + \varepsilon\eta(t)) \ .$$

Substituting $x(t) + \varepsilon\eta(t)$ for $x(t)$ in the functional $\mathcal{S}(x(t))$, the result is a function of ε:

$$\mathcal{S}_\varepsilon := \mathcal{S}(x(t) + \varepsilon\eta(t)).$$

From now on, I have dropped the dependence on t and abbreviated $\mathcal{L}(t, x^{(3)}(t) + \varepsilon\dot{\eta}^{(3)}(t)) := \mathcal{L}_\varepsilon$ to ease the notation. Since the functional $\mathcal{S}(x(t))$ has a minimum for $x(t) = x^*(t)$, the function $\mathcal{S}(\varepsilon)$ has a minimum at $\varepsilon = 0$, and thus

$$\left.\frac{\mathrm{d}\mathcal{S}_\varepsilon}{\mathrm{d}\varepsilon}\right|_{\varepsilon=0} = \int_{t_i}^{t_f} \left.\frac{\mathrm{d}\mathcal{L}_\varepsilon}{\mathrm{d}\varepsilon}\right|_{\varepsilon=0} dt = 0$$

Then, solving the system for our case, we have that

$$\left.\frac{\mathrm{d}\mathcal{S}_\varepsilon}{\mathrm{d}\varepsilon}\right|_{\varepsilon=0} = \int_{t_i}^{t_f} \left.\frac{d(||x^{(3)}(t) + \varepsilon\eta^{(3)}(t)||)^2}{d\varepsilon}\right|_{\varepsilon=0} dt = 0$$

Proceeding with the computations,

$$2\int_{t_i}^{t_f} \left(\ || \ x^{(3)}(t) + \varepsilon\eta^{(3)}(t) \ || \ \right) \eta^{(3)}(t) \Big|_{\varepsilon=0} dt = 2\int_{t_i}^{t_f} ||x^{(3)}(t)|| \ \eta^{(3)}(t) dt = 0$$

Then, we must solve

$$\int_{t_i}^{t_f} ||x^{(3)}(t)|| \ \eta^{(3)}(t) dt = 0$$

Using integration by parts, we have

$$\int_{t_i}^{t_f} ||x^{(3)}(t)|| \ \eta^{(3)}(t) dt = ||x^{(3)}(t)|| \ \eta^{(2)}(t) \Big|_{t_i}^{t_f} - \int_{t_i}^{t_f} ||x^{(4)}(t)|| \ \eta^{(2)}(t) dt = 0$$

Since $\eta(t_i) = \eta(t_f) = 0$, $\eta^{(2)}(t_i) = \eta^{(2)}(t_f) = 0$.

$$\int_{t_i}^{t_f} ||x^{(4)}(t)|| \ \eta^{(2)}(t) dt = 0.$$

Where $x^{(4)}$ is the 4^{th} derivative of $x(t)$. Using integration by parts again,

$$\int_{t_i}^{t_f} ||x^{(4)}(t)|| \ \eta^{(2)}(t) dt = ||x^{(4)}(t)|| \ \dot{\eta}(t) \Big|_{t_i}^{t_f} - \int_{t_i}^{t_f} ||x^{(5)}(t)|| \ \dot{\eta}(t) dt = 0$$

Following the same argument as before, we end up having

$$\int_{t_i}^{t_f} ||x^{(5)}(t)||\ \dot{\eta}(t)dt = 0.$$

Integrating by parts one last time, we end up having

$$\int_{t_i}^{t_f} ||x^{(6)}(t)||\ \eta(t)dt = 0.$$

Since it must hold for any function $\eta(t)$, the solution to the minimization is

$$x^{(6)}(t) = 0$$

which is the same as Eq. (11).

3.2.4 Trajectory generation

Now that we have an solution for the minimization of the Lagrangian (10), the next step is to compute the trajectories emerging from it. First, we see that Eq. (11) has the general solution (for polynomials)

$$x(t) = a_0 + a_1 t + a_2 t^2 + a_3 t^3 + a_4 t^4 + a_5 t^5 = v(t)^T \mathbf{a} \tag{13}$$

with $v(t) = (1, t, t^2, t^3, t^4, t^5)$ and $\mathbf{a} = (a_0, a_1, a_2, a_3, a_4, a_5)$. The solution has derivatives

$$\begin{aligned} \dot{x}(t) &= a_1 + 2a_2 t + 3a_3 t^2 + 4a_4 t^3 + 5a_5 t^4 \\ \ddot{x}(t) &= 2a_2 + 6a_3 t + 12a_4 t^2 + 20a_5 t^3 \end{aligned}$$

where $\dot{x}(t)$ is the velocity and $\ddot{x}(t)$ the acceleration of the system. To find the coefficients $\mathbf{a}$, we must use the boundary conditions. We define μ as the vector containing the position, velocity and acceleration at the boundaries ($t = t_i, t_f$), which correspond to initial and final time of the trajectory, respectively. Specifically, the structure of μ is

$$\mu = (x(t_0), \dot{x}(t_0), \ddot{x}(t_0), x(t_f), \dot{x}(t_f), \ddot{x}(t_f))\ .$$

Then, we have a set of 6 linear equations $\mu = M(t_0, t_f)\mathbf{a}$, with matrix:

$$M(t_0, t_f) = \begin{pmatrix} 1 & t_0 & t_0^2 & t_0^3 & t_0^4 & t_0^5 \\ 0 & 1 & 2t_0 & 3t_0^2 & 4t_0^3 & 5t_0^4 \\ 0 & 0 & 2 & 6t_0 & 12t_0^2 & 20t_0^3 \\ 1 & t_f & t_f^2 & t_f^3 & t_f^4 & t_f^5 \\ 0 & 1 & 2t_f & 3t_f^2 & 4t_f^3 & 5t_f^4 \\ 0 & 0 & 2 & 6t_f & 12t_f^2 & 20t_f^3 \end{pmatrix}\ .$$

We can obtain the parameters as a function of the boundary conditions:

$$\mathbf{a} = M(t_0, t_f)^{-1}\mu\ . \tag{14}$$

Then, we could use any software program to compute the inverse of M. In order to optimize computational power, since the computational complexity used to invert matrices by any programming software is very high compared to analytical solutions ($\mathcal{O}(n^3)$ and $\mathcal{O}(n)$, respectively), we can derive an analytical expression

of the inverse of the matrix M using *blockwise inversion* [48, 49]. This process is shown in Appendix B. Moreover, we set $t_0 = 0$ for convenience. The inverse of M (with $t_0 = 0$) in terms of t_f is

$$M(t_0 = 0, t_f)^{-1} = \begin{pmatrix} 1 & 0 & 0 & 0 & 0 & 0 \\ 0 & 1 & 0 & 0 & 0 & 0 \\ 0 & 0 & 1/2 & 0 & 0 & 0 \\ -10/t_f^3 & -6/t_f^2 & -3/2t_f & 10/t_f^3 & -4/t_f^2 & 1/2t_f \\ 15/t_f^4 & 8/t_f^3 & 3/2t_f^2 & -15/t_f^4 & 7/t_f^3 & -1/t_f^2 \\ -6/t_f^5 & -3/t_f^4 & -1/2t_f^3 & 6/t_f^5 & -3/t_f^4 & 1/2t_f^3 \end{pmatrix} .$$

In our case, we have that the final time t_f is the Movement Time (MT), $t_f = MT$. For the initial trajectory, we can set the following boundary conditions:

$$\mu = (0, 0, 0, \pm 75\text{pixels}, 0, 0)$$

For the update, we set the following ones:

$$\mu = (x(t_{2nd}), \dot{x}(t_{2nd}), \ddot{x}(t_{2nd}), \pm 75\text{pixels}, 0, 0)$$

Where $x(t_{2nd}), \dot{x}(t_{2nd}), \ddot{x}(t_{2nd})$ are the position, velocity and acceleration of the system at time $t = t_{2nd} = t_{updt} + t_{1st}$, which are known. t_{1st} is the time at which the execution of the first response has begun. Recall the meaning of t_{updt} in Remark 3.4, i.e. the difference in time between readouts. Therefore, going back to Eq. (14), $\mathbf{a}$ will only depend on MT:

$$\mathbf{a} = M(0, MT)^{-1}\mu \, .$$

Finally, the trajectory from Eq. (13) is given by

$$x(t) = v(t)^T M(0, MT)^{-1}\mu$$

and only depends on MT.

Remark 3.9. The trajectory generation does not have any related free parameter.

3.2.5 Qualitative comparison with data

In this section, my objective is to compare the trajectories derived using different magnitudes for minimization (i.e. changing r in (12)), and assert wether the minimum jerk trajectories are a good approximation of rats' movements. The process of computing the trajectory for any r is similar as for $r = 3$ in section 3.2.4. First, one has the polynomial solution of (12)

$$x(t) = a_0 + a_1\, t + a_2\, t^2 + \cdots + a_{2r-1}\, t^{2r-1} = v(t)^T \mathbf{a} \, , \tag{15}$$

where $v(t) = (1, t, t^2, \ldots, t^{2r-1})$ and $\mathbf{a} = (a_0, a_1, a_2, \ldots, a_{2r-1})$. Moreover, we can easily compute the corresponding first $(r-1)_{th}$ time derivatives of $x(t)$. Combining these derivatives and the solution of the

trajectory $x(t)$, we can compute M, which will be a $2r \times 2r$ matrix of the form

$$M(t_0, t_f) = \begin{pmatrix} 1 & t_0 & t_0^2 & \dots & t_0^{2r-2} & t_0^{2r-1} \\ 0 & 1 & 2t_0 & \dots & (2r-2)\, t_0^{2r-3} & (2r-1)\, t_0^{2r-2} \\ & & & \dots & & \\ 0 & 0 & 0 & \dots & \frac{(2r-2)!}{(r-1)!}\, t_0^{r-1} & \frac{(2r-1)!}{r!}\, t_0^{r} \\ 1 & t_f & t_f^2 & \dots & t_f^{2r-2} & t_f^{2r-1} \\ 0 & 1 & 2t_f & \dots & (2r-2)\, t_f^{2r-3} & (2r-1)\, t_f^{2r-2} \\ & & & \dots & & \\ 0 & 0 & 0 & \dots & \frac{(2r-2)!}{(r-1)!}\, t_f^{r-1} & \frac{(2r-1)!}{r!}\, t_f^{r} \end{pmatrix} .$$

Therefore, since we need the boundary conditions for the position and the first $r-1$ derivatives, μ will be a vector of length $2r$, structured as

$$\mu = (x(t_0), \dot{x}(t_0), \dots, x^{(r-1)}(t_0), x(t_f), \dot{x}(t_f), \dots, x^{(r-1)}(t_f)) .$$

Using (14) on (15), we can express the final trajectory as

$$x(t) = v(t)^T M(t_0, t_f)^{-1} \mu .$$

With this, we can compute the trajectories emerging from minimizing the r_{th} time derivative of position along the trajectory. The next step is to compare them with the trajectories from experimental rat data.

Minimum-jerk trajectories. For the minimum-jerk trajectories, shown in Fig. 3.3 conditioned by MT magnitude, we can see that both acceleration and velocity evolve and end in a smooth way, which resembles a natural movement.

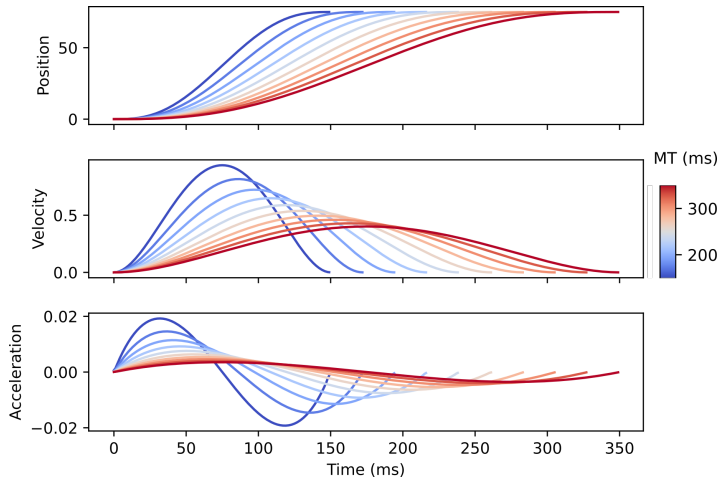

Figure 3.3: Minimum jerk trajectories. Magnitudes for position, velocity and acceleration are pixels, pixels/s and pixels/s^2, respectively.

Minimum-acceleration trajectories. Given that we are minimizing the acceleration, we are working with $r = 2$. Following the trajectory generation process for any r explained above, in this case we have a square

matrix M with dimensions $2r \times 2r = 4 \times 4$. In this case, $\mu = (x(0), \dot{x}(0), x(t_f), \dot{x}(t_f)) = (0, 0, \pm 75, 0)$. The trajectories are shown in Fig. 3.4, where we can observe that the velocity and acceleration look like an approximation of the minimum-jerk trajectories, but both end abruptly, which is unrealistic, since it has been seen that naturalistic movements are smooth [40, 41].

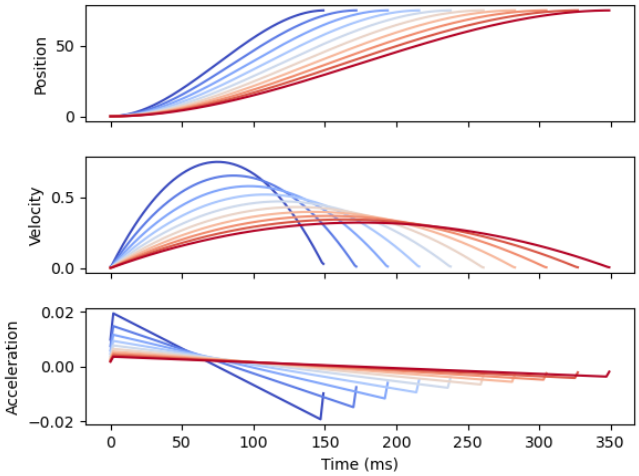

Figure 3.4: Minimum acceleration trajectories. Magnitudes for position, velocity and acceleration are pixels, pixels/s and pixels/s^2, respectively.

Minimum-span trajectories. In the case of the minimum-span trajectories, we are minimizing the fourth derivative of position w.r.t. time ($r = 4$). Therefore, we have a $8x8$ square matrix M. And $\mu = (x(0), \dot{x}(0), \ddot{x}(0), x^{(3)}(0), x(t_f), \dot{x}(t_f), \ddot{x}(t_f), x^{(3)}(t_f)) = (0, 0, 0, 0, \pm 75, 0, 0, 0)$. The trajectories are shown in Fig. 3.5, where we can observe that the velocity and acceleration end abruptly, a bit unrealistic, as discussed before.

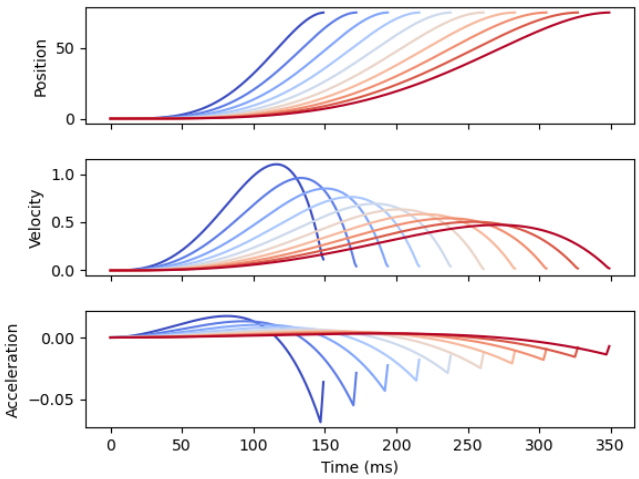

Figure 3.5: Minimum span trajectories. Magnitudes for position, velocity and acceleration are pixels, pixels/s and pixels/s^2, respectively.

Real data. If we then compare the simulated results with trajectories from experimental rat data (shown in Fig. 3.6), we see that the best approximation is the one from the minimum jerk, in Fig. 3.3, since velocity and acceleration from data trajectories also end smoothly. In addition, the polynomials derived for the minimum-jerk trajectories are qualitatively similar to the rats' movement and its derivatives. Therefore, we can say that the results from previous studies regarding humans [40, 41] also explains rat movement, which must follow smooth trajectories by minimizing the jerk.

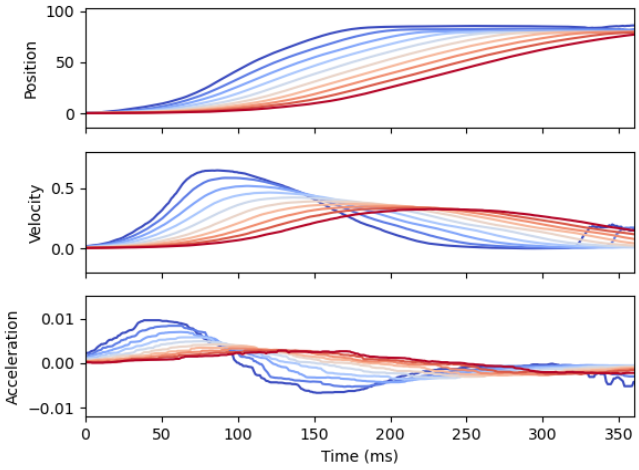

Figure 3.6: Rat trajectories conditioned to MT. Magnitudes for position, velocity and acceleration are pixels, pixels/s and pixels/s^2, respectively.

3.3 Bridge - Modelling the Motor Time

At this point, we have a decoupled system formed by a sensory integration model and a trajectory generation stage, so we must set a link between them. Since the trajectory generation only receives as input the MT, our scope will be to translate the decision variable X_t from the sensory integration module into it. We assume a initial MT value that should be related to trial index (TI) with some noise $\mathcal{G}$, given by

$$\mathrm{MT}_{init} = p_{MT,0} + p_{MT,1}\ \mathrm{TI} + p_N\ \mathcal{G}(0,1) \tag{16}$$

where $p_{MT,0}$, $p_{MT,1}$ are free parameters corresponding to the linear relationship of the motor time with the trial index, and p_N is a free parameter corresponding to the weight of the noise $\mathcal{G}$, which follows a Gumbel distribution. The Gumbel distribution is a popular and asymmetric distribution, used because it is right skewed by definition, and since the MT distribution from experimental rat data is right-skewed too (Fig. 2.6), the shape of the noise is similar to the data. On the other hand, the relation between the MT and the trial index has been found in experimental data from rats (Fig. 2.6), where rats are more tired as the trial index is bigger, so movements become slower.

After computing the initial MT_{init}, we must introduce a dependence of the decision variable into the MT. To do so, we apply two mappings. The first one, corresponding to the first readout, considers the absolute value of the decision variable ($X_{t_{1st}}$) at the first readout, i.e. when $t = t_{1st}$; as a measure of confidence due to accumulated decision evidence:

$$\mathrm{MT}_{1st} = \mathrm{MT}_{init} - p_{1st}|X_{t_{1st}}|\ .$$

This way, we get that the MT has a negative linear relationship with the absolute value of both combined prior and stimulus evidence, while maintaining a positive relationship with trial index. If stimulus is not integrated (proactive responses, mainly in short RT) the prior will be the main contributor to the MT reduction, and the stimulus will affect mainly in the second readout. Recall that for rats the negative relationship studied was with the congruency of these variables with the final response. Then, given that rats can accelerate (confirming), decelerate (slowing, less sure) and change their mind, we need to have a mapping for the second readout that permits all cases. Recall that the second readout is at t_{updt} from the first one, and is subtracted because the rat has moved t_{updt} seconds, therefore

$$\mathrm{MT}_{2n} = \mathrm{MT}_{1st} - t_{updt} - \mathrm{sgn}(X_{t_{1st}})\, p_{2nd}(X_{t_{2nd}} - X_{t_{1st}})\,. \tag{17}$$

This way, if the evidence at the second readout is greater than at the first one, the rat will accelerate (MT will be reduced). Also if the evidence at the second readout is smaller than the first one or changes it's sign, there will be a slowing in the velocity, i.e. MT will be increased. Summary of possible interesting cases:

- Prior congruency
  - Congruent: Decision Variable (DV) is pointing in the same direction in both readouts, MT is more likely to be reduced.
  - Incongruent: DV points to different directions in both readouts, MT is most likely to be augmented.

  Therefore showing the same relationship as in rats (Fig. 2.3).
- Stimulus congruency
  - Congruent: stimulus is well integrated, leading to larger values of DV and thus smaller values of MT.
  - Incongruent: stimulus is not well integrated/processed due to lack of time or difficulty in the stimulus itself. The response is most likely to be given by the prior or by noise, which tends to zero due to the leak and therefore, MT is most likely to be augmented.

On the other hand, if the prior is very high but incongruent with the final response, the first response is most likely to be given by the prior magnitude, then as the stimulus arrives, the response is changed and therefore the Decision Variable (DV) points to the other side. Hence, the MT will be enlarged when there is incongruency between stimulus and prior (most likely reversals). To sum up, we have seen that the same negative linear relationships between MT and prior and stimulus congruency shown in experimental data from rats (Fig. 2.3, 2.4 respectively) are present in the model by the mappings defined in this section.

3.4 The full model

A schematic of the full model is shown in Fig. 3.7. The model starts with the parallel stochastic integration (evidence and action), and the first process that reaches its respective bound triggers a response towards the side where the evidence is pointing at (left or right). In the schematic (Fig. 3.7 top left), there is a proactive response where action reached first the bound, and the first decision is taken considering the sign of the decision variable, shown as a collapse of the bounds at the point where the decision variable is

when action triggered the response. Then, no matter which process triggered the response, a first MT_{init} is computed following Eq. (16), and a trajectory $x(t)$ is generated (Fig. 3.7, center) as

$$x(t) = v(t)^T M(0, MT_{init})^{-1} \mu \quad \text{with } \mu = (0, 0, 0, \pm 75\text{pixels}, 0, 0) \ .$$

Then, the sensory integration continues up to $t_{2nd} = t_{1st} + t_{updt}$, where t_{1st} is the time at which the execution of the first response has begun; therefore t_{2nd} is the time at which the second readout affects the trajectory, i.e. the time of the second readout plus t_{eff}. At this point, a second trajectory (Fig. 3.7, right) is planned with a movement time MT^* computed following Eq. (17), leading to acceleration, slowing or trajectory reversal. This trajectory has the initial conditions on the point where the update happens, and it is computed as

$$x(t) = v(t)^T M(0, MT^*)^{-1} \mu^* \quad \text{with } \mu^* = (x(t_{2nd}), \dot{x}(t_{2nd}), \ddot{x}(t_{2nd}), \pm 75\text{pixels}, 0, 0) \ .$$

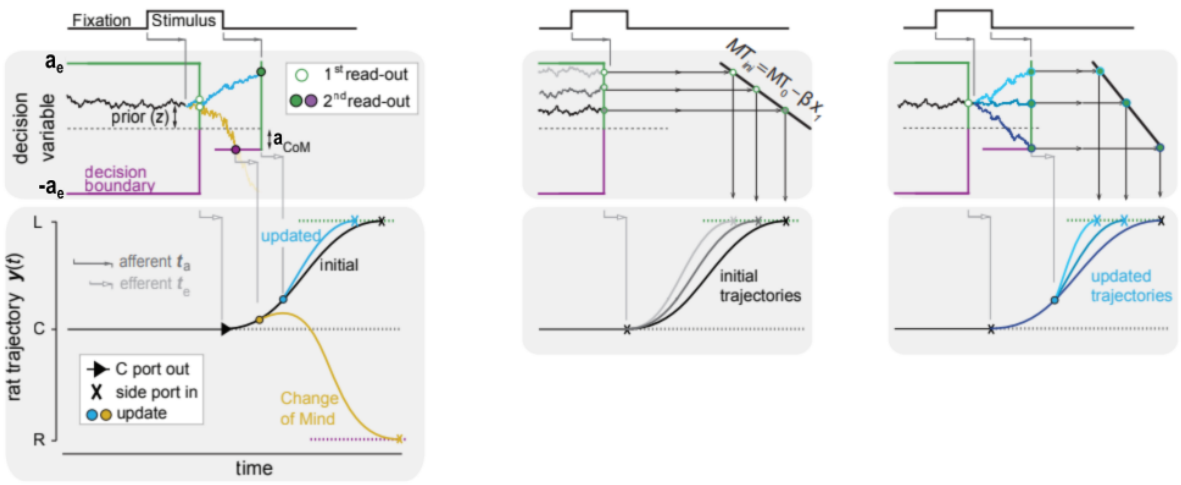

Figure 3.7: The whole serial model schematic. Left, top: decision variable integration example for a proactive response. Left, bottom: rat trajectory and its possible updates depending on the decision variable. Center: linear mapping for the first trajectory. Right: linear mapping for the updated trajectory.

3.5 Free parameters summary

We have a total of 16 free parameters, separated in 3 categories, depending on which variable of the model are explicitly affecting.

- Decision variable
  - p_s: weight of the stimulus, how much the stimulus s affects the integration drift ν, defined as $\nu = p_s \, s$.
  - p_z: weight of the prior, how much the prior z affects the initial bias Z, defined as $Z = p_z \, z$.

  - a_e: bounds for evidence integration. Once the integrator reaches the bound, a reactive choice is started.
  - t_{aff}: afferent time, time it takes for the stimulus to reach the corresponding sensory processing region in the brain.
  - t_{eff}: efferent time, time it takes for the brain to send a motor action and for the rat to start its execution.
  - λ: proportion of leak, in other words, proportion of the previous time-step that is forgotten.
  - a_{CoM}: bound for Change of Mind. Once the first response is triggered, if the integration of the decision variable reaches the bound, the response will be flipped.

- Action variable
  - $p_{A,0}$: intercept of the linear relationship between the action drift ν_a and the trial index.
  - $p_{A,1} > 0$: slope of the linear relationship between the action drift ν_A and the trial index. Recall that $\nu_A = p_{A,0} + p_{A,1} \cdot \text{TI}$.
  - a_A: bound for action variable. Once the integrator reaches the bound, a response is triggered.
  - t_A: time offset for action, delay in the beginning of the integration of the action variable.

- Movement Time
  - $p_{MT,0}$: intercept of the linear relationship between MT and trial index in the first read-out.
  - $p_{MT,1}$: slope of the linear relationship between MT and trial index in the first read-out.
  - p_N: noise amplitude of the linear relationship between MT and trial index in the first read-out.
  - p_{1st}: weight of the absolute value of the decision variable to reduce the MT in the first read-out.
  - p_{2nd}: weight of the difference of the decision variable between the second and the first read-out.

3.6 Grid Search fitting

As a first approach, I did a brute force (BF) search in the 16-dimensional space of parameters Θ. To do so, I created a grid in Θ and I simulated the model with all the combinations of parameters possible in this grid. Then, I chose the set of parameters θ_{BF} that better represented the rats' data, qualitatively (i.e. by visual inspection). Finally, I fixed this set of parameters θ_{BF} and I simulated the model for each rat's experimental conditions and averaged the results across all simulated rats. Then, I performed the same analysis done to experimental rat data (Section 2) to the model simulations. First, we see that the dependencies on the choice with the sources of information is well captured (Fig. 3.8), where the matrix is qualitatively similar to the one from experiments with rats (Fig. 2.1).
In addition, movement times (MT) and trajectories have a qualitative similar shape and dependencies with the experimental variables (Fig. 3.9). In addition, we can see that the trajectories diverge earlier when conditioning on prior than when conditioning on stimulus, also seen in experimental data.
Moreover, the simulated reversal trajectories (Fig 3.10) are similar to the ones from rats (Fig. 2.8). However, in general rats spend more time at $y = 0$, due to spatial constraints imposed by the dimensions of the set-up, rats have to move backwards (at the same $y = 0$) until they can turn to their first response side. Even the relations of the probability of reversal and the experimental variables are well captured (Fig. 3.11), compared to rats (Fig. 2.9).

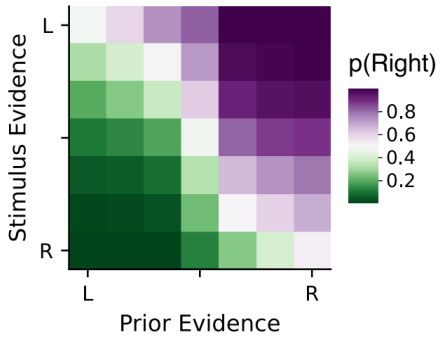

Figure 3.8: Probability of rightwards response matrix for the model.

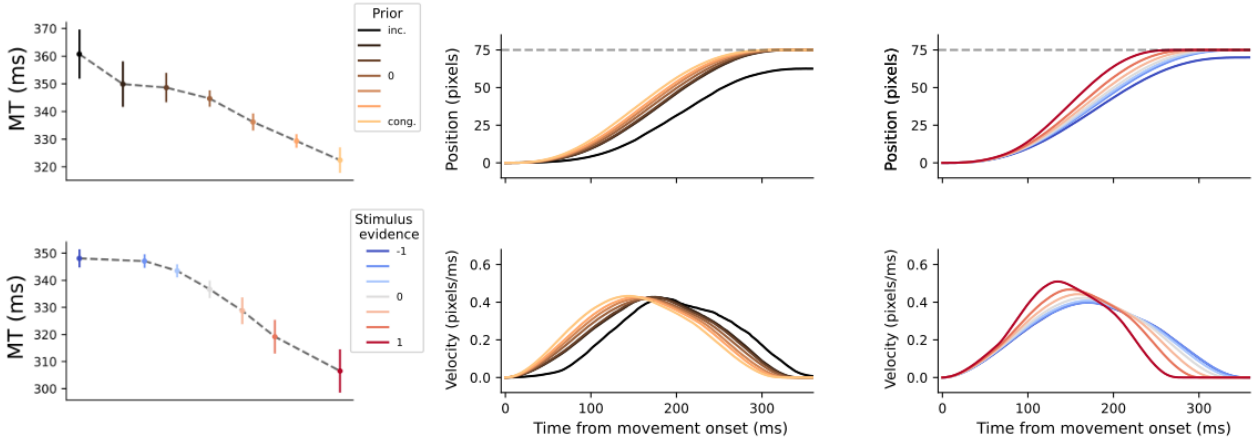

Figure 3.9: Top Left: simulated MT conditioned to prior evidence. Bottom Left: simulated MT conditioned to stimulus evidence. For center and right, top, bottom: trajectories and velocities conditioned on prior and stimulus evidence, respectively.

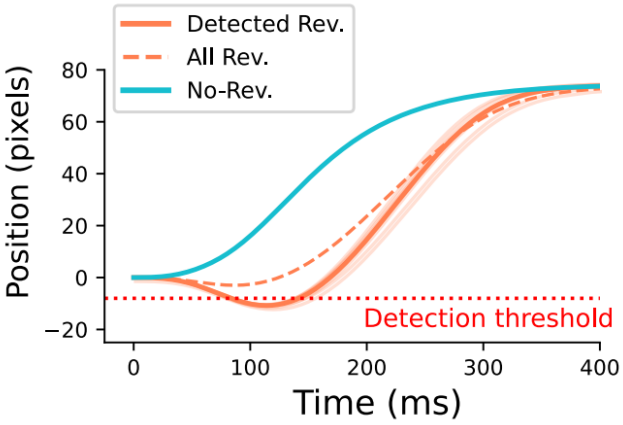

Figure 3.10: Average trajectories for detected reversals, non-reversals and non-detected reversals.

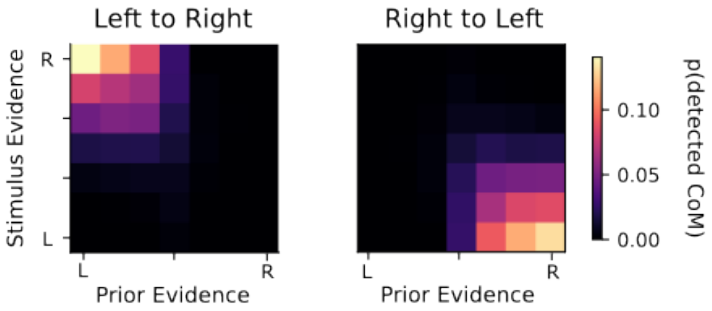

Figure 3.11: Left and Right: Simulated probability of reversal (i.e. detected CoM) as a function of both prior and stimulus, conditioned to Right and Left responses, respectively.

To sum up, we have seen that the model can capture and explain rat behavior, the dependencies of their movements with the sensory information and their choice. Now, given the potential of the model, we must find a robust way to fit the model to each rat.

4. Model fitting

The Grid Search fitting is very limited when it comes to find the combination of parameters of the model which best describe the data, because its computational complexity increases rapidly and the parameter space Θ is not entirely searched. Therefore, I wanted a more systematic and rigorous fitting method that could cover a greater part of Θ. The classical approaches use the likelihood, which is the joint probability of the observed data viewed as a function of the parameters of the model, i.e. how probable is that the model returns the real data X given the parameters θ, expressed as $p(X \mid \theta)$. Given that we cannot have an explicit expression for the likelihood of the model, we are forced to approximate it by simulations. However, since we have continuous experimental conditions (prior evidence and trial index), we need a lot of computational power to approximate the likelihoods by simulating many times the model at each condition. As a consequence, I had to search for some tools to approximate it.

4.1 Mixed Neural Likelihood Estimation

The tool that I used was Mixed Neural Likelihood Estimation (MNLE), which is a novel approach to extract an approximation of the likelihood [50]. The goal is to acquire a numerical approximation of the likelihood of some data given certain parameters, using simulation-based inference [51], since no analytical expression can be used for the whole model. This specific method is based on density estimation, which addresses the problem of discovering structure (likelihood) from data in an unsupervised manner. A density function is a complete description of the joint statistical properties of the data, and in that sense a model of the density function can be viewed as a model of data structure. As such, a model of the density function can be used in a variety of downstream tasks that involve knowledge of data structure, such as inference [52]. More specifically, MNLE is based on training a neural network to predict the approximate likelihood conditioned on the model parameters [52, 53]. To do so, they use a certain architecture of neural network, which is the neural density estimator, i.e. a density estimator based on neural networks [54], trained on model simulations to emulate the simulator (i.e. the model), which is designed to capture both the continuous (e.g., reaction times and movement times) and discrete (choices) likelihoods. The likelihoods of the emulator can then be used to perform Bayesian parameter inference on experimental data.
Our application. The objective will be fitting the choice and the RT and MT distributions. The workflow is shown in Fig. 4.1. First, we do a number of simulations N_{sim} (the more the better), with different sets of parameters θ distributed in a defined closed region of the 16-dimensional parameter space Θ, varying experimental conditions (stimulus, prior, trial index) too. Then, we end up with a matrix X_{sim} with N_{sim} rows and 3 columns of simulated data: RT, MT and choice; shown in left panel of Fig. 4.1. Then, the same parameters and experimental conditions are used as inputs for the network, with the matrix X_{sim} as output. The network is made of two concatenated networks, the first one for discrete outputs (choice), whose output is used as input for the second one, with continuous output (RT, MT), shown in the central panel of Fig. 4.1. After having trained the network for N_{sim} different sets of parameters and experimental conditions, the joint likelihood $p(\text{RT, MT, choice } |\theta, \text{prior, stimulus})$ (θ represents a fixed set of parameters) can be computed for any value of RT, MT, choice, as shown in the right panel of Fig. 4.1. This way, we can express the likelihood as $\mathcal{L}_{MNLE}(X_{data}|\theta)$ and use optimization algorithms to get the combination of parameters that maximizes this likelihood when experimental rat data is presented. In our case, I trained the network with $2 \cdot 10^6$ simulations. The training process lasted roughly 3 days, therefore all the steps and changes had to be done carefully.

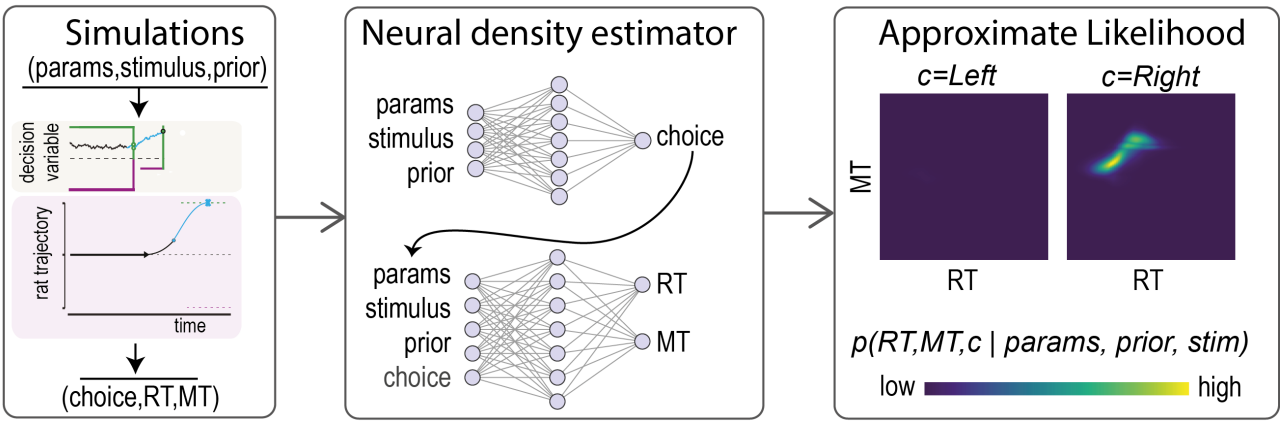

Figure 4.1: Schematic of likelihood approximation using neural density estimators.

4.1.1 Model vs MNLE

We need to see if the network approximates correctly the likelihood of the model. To do so, I fixed a set of parameters θ^* and defined 6 different experimental conditions. Then, I simulated the model $5 \cdot 10^5$ times and extracted the likelihood matrices conditioned to MT, RT and choice. Then, I computed the likelihood returned by the network in the same type of trials, and plotted it as a contour on top of the previous matrices (Fig. 4.2).

We can see that the likelihood approximates quite well for the network trained with $2 \cdot 10^6$ trials, for different experimental conditions. However, there are some mismatches in the shape of the likelihood that could lead to fitting errors (i.e. increasing N_{sim}). This could be solved by training the network with more simulated trials. Regarding the probability of choice (Fig. 4.2, black bars), we see that it approximates quite well, even though there are some differences.

Since the network's inputs are the parameters and experimental conditions and the outputs the variables wanted (MT, RT, choice), the likelihood must be defined for all kind of trials. Nevertheless, there are some trials where the likelihood can not be expressed with the network. Data trials with RT < 0, called fixation breaks, have no movement time nor choice associated, and the network cannot give a likelihood of empty values of the variables. Therefore, the MNLE approach only gives the approximated likelihood for trials with $RT > 0$, and we need to find a way to work with fixation breaks.

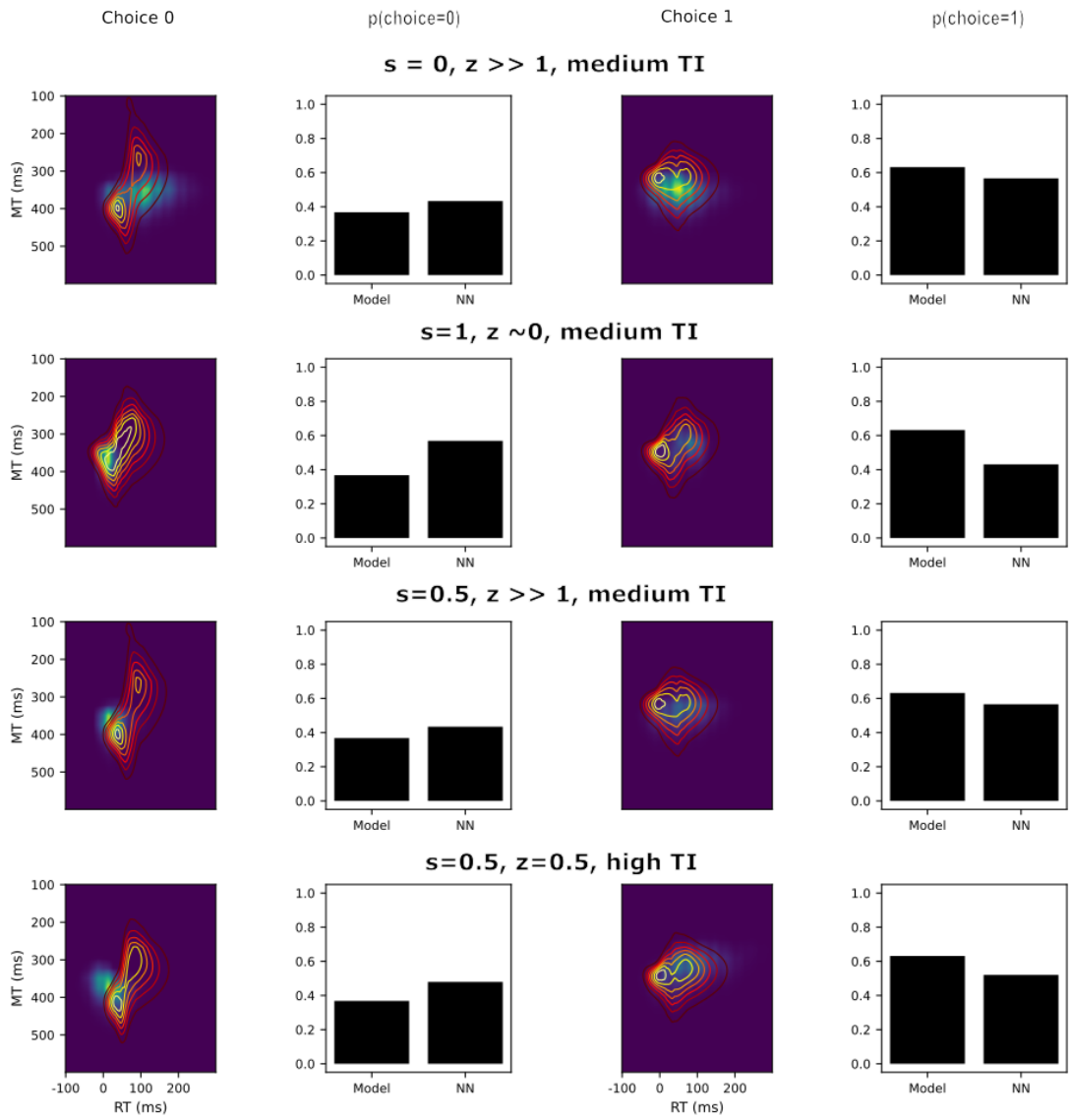

Figure 4.2: Likelihood for different trials (s is stimulus, z is prior evidence and TI is trial index). Matrices in first and third column: likelihood of the model. Contour in first and third column, in red/yellow gradient: estimated likelihood from the network. Bars in second and fourth column: probability of choice.

4.2 Fixation Breaks Likelihood

Fixation Breaks are the trials where the rat leaves the central port before the stimulus onset, breaking the fixation section (i.e. $RT < 0$). These trials have no associated movement time nor choice in the data. Therefore, we can fit the reaction times smaller than zero considering that the unique source generating them is the Action Initiation process. In this case, we should derive the probability density distribution of the first-hitting time of this drifted Wiener process. To do so, we use the previously derived probability density function (p_A) for the first time passage of a Wiener process (i.e. our reaction time, expressed by

t) with one bound [21], conditioned by the parameters. In our paradigm, the equation is

$$p_{\mathrm{A}}(t|\nu_{\mathrm{A}}, a_{\mathrm{A}}, \hat{t}_{\mathrm{A}}) = a_{\mathrm{A}} \cdot \frac{1}{\sqrt{2\pi \cdot (t-\hat{t}_{\mathrm{A}})^3}} \cdot \exp\left(-\frac{\nu_{\mathrm{A}}^2}{2} \cdot \frac{[(t-\hat{t}_{\mathrm{A}}) - a_{\mathrm{A}}/\nu_{\mathrm{A}}]^2}{(t-\hat{t}_{\mathrm{A}})}\right) ,$$

where $\hat{t}_{\mathrm{A}} = t_A + t_{eff}$, a_A is the bound of the action integration and ν_A the drift, with $\nu_A = p_{A,0} + \mathrm{TI} \cdot p_{A,1}$. The probability density function follows a Wald distribution (or inverse Gaussian distribution). Then, we can express the likelihood of a reaction time given a set of parameters θ as $\mathcal{L}_{FB}(\mathrm{RT}|\,\theta) = p_{\mathrm{A}}(\mathrm{RT}|\,\theta)$.

4.3 Overall likelihood

Therefore, our likelihood is defined as a piecewise function

$$\mathcal{L}(x_i|\,\theta) = \begin{cases} \mathcal{L}_{MNLE}(x_i|\,\theta) & \text{if } RT_i > 0 \\ \mathcal{L}_{FB}(RT_i|\,\theta) & \text{otherwise} \end{cases}$$

for all $i = 1, \ldots, N_{data}$, where $x_i = \{MT_i, RT_i, \mathrm{choice}_i\}$ and N_{data} is the number of trials from the experimental data. Indeed, the overall likelihood will be

$$\mathcal{L}(X_{data} \mid \theta) = \prod_{i=1}^{N_{data}} \mathcal{L}(x_i \mid \theta) .$$

Since the sum is computationally more efficient than a product, we define the log-likelihood as

$$\log \mathcal{L}(X_{data} \mid \theta) = \sum_{i=1}^{N_{data}} \log \mathcal{L}(x_i \mid \theta) ,$$

by using the basic properties of the logarithm. Note that the extremum is not altered with this transformation since the logarithm is a monotonically increasing function. Since we want the maximum of the likelihood, given by a set of parameters $\hat{\theta}$, we have to define an optimization problem. Since most of the optimizers work finding minima, we can define the optimization problem as the minimization of the negative log-likelihood

$$\hat{\theta} = \arg\min_{\theta \in \Theta} \sum_{i}^{N} -\log\left(\mathcal{L}(x_i|\theta)\right) ,$$

where N is the number of trials to evaluate ($N \leq N_{data}$) and Θ the 16-dimensional parameter space.

4.4 Optimizer

For the optimization, I used Bayesian Adaptive Direct Search (BADS) [55], which is a fast hybrid Bayesian optimization algorithm designed to solve difficult optimization problems. BADS is mainly used when no gradient information is available [56], and the objective function is non-analytical or noisy, for example evaluated through numerical approximation, which is our case. Using the likelihood described above, the optimizer converges for all rats after roughly 6 hours, therefore, all the fitting process has a huge limitation regarding computational time and rapid workflow.

5. Results

In this section, I will analyze the results of the model, fitted by the method explained in section 4.

5.1 Fitting results

Once the model is fitted, we have a set of parameters θ_i for each rat, $i = 1, \dots, 15$. Then, I run the model to produce simulated trials and proceed with the same analysis as in Section 2 for experimental data from rats.

5.1.1 Choice

We can see that the model used both sources of information (prior and stimulus evidence) for the choice (Fig. 5.1), as rats (Fig. 2.1). Nevertheless, we see that in average the prior has smaller effect on the fitted model, since the matrix is not as diagonal as for rats (i.e. stimulus is more important for the decision); which may be because the leak is causing the disappearance of the prior as time goes by. I have made this hypothesis because the fitted leak parameter is near the respective upper bound in Θ for all rats (Appendix C, Fig. C.1, bottom left).

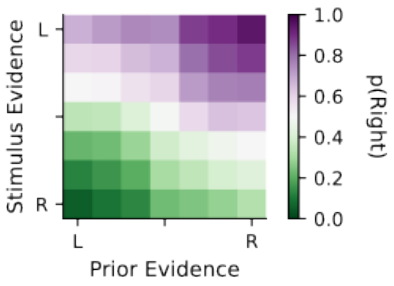

Figure 5.1: Probability of right choice matrix conditioned to stimulus and prior evidence for the fitted model.

5.1.2 MT and trajectories

The duration of model trajectories depended both on the movement time planned at the initial read-out and on its update at the second read-out. Both of these calculations depend on the decision variable, which summarizes both the prior and sensory information. For this reason the model should account for the dependence of the duration of the rats' trajectories on both prior and sensory information (Fig. 5.2). However, we see that there is no relationship with the prior evidence (Fig. 5.2, left). The fitting method is not fitting well the trials without stimulus (called silent trials), which are the ones used to evaluate the influence of the prior. Indeed, these silent trials are only a small percentage and thus it might be difficult for the model to fit them. This may be because in these trials the prior is the unique magnitude affecting the sensory integration (there is no stimulus), combined with the leak. Therefore, it might happen that the initial magnitude (prior) is reduced to zero because of the leak, since this parameter is very big, and

then the effect of the prior gets reduced. In addition, if the weight of the decision variable on the MT at the first readout (i.e. p_{1st}) is small, the prior has no effect on the MT.
Another cause could be that the optimizer encounters a minimum, with the approximated likelihood from the network, where the fitting of the MT distribution with the trial index regression with noise is sufficient (Eq. (16), Fig. 5.4). Then, the effects of prior can get reduced, because the related parameter is just big enough to fit the choice and the MT is already fitted.

On the other hand, the model captures the negative linear relationship between the MT and the stimulus (Fig. 5.2, right) seen in data (Fig. 2.4), with very similar values on the MT.

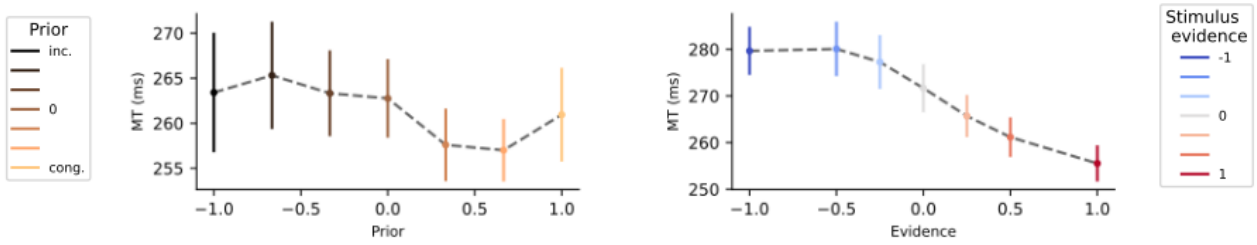

Figure 5.2: Simulated MT conditioned to prior and stimulus evidence.

Regarding the average trajectories, we have the same effect as before, the prior has no discernible effect, whereas the stimulus has, even though it is small.

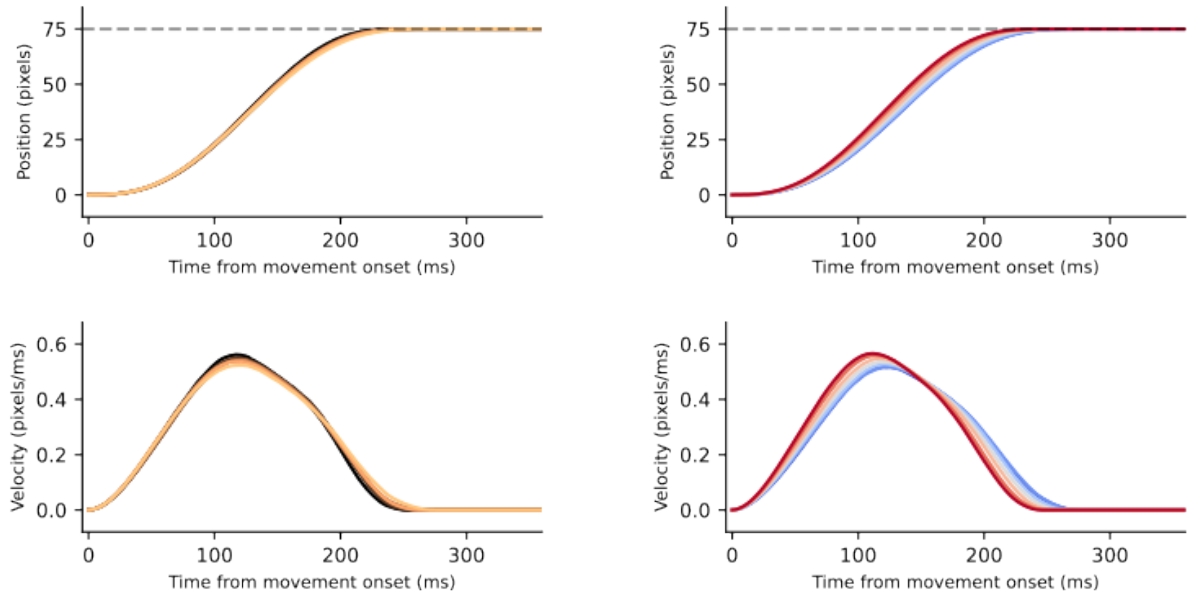

Figure 5.3: Trajectories (top) and velocities (bottom) conditioned to prior evidence (left) and stimulus evidence (right, trials for RT $<$ 50 ms).

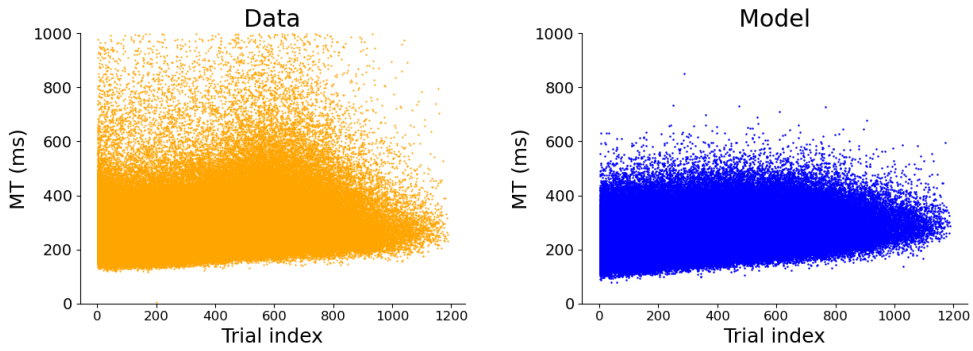

Figure 5.4: MT vs trial index for Data (left) and Model (right), for three rats to simplify the plot.

5.1.3 Single rat simulations

The bad fitting regarding the prior effect on the simulated MT and trajectories is seen only when averaging across rats. Some simulated rats individually show the expected dependencies (Fig. 5.5). We see that for this simulated rat, all incongruent prior evidences are most likely to cause reversals, even if there is no stimulus. That may be because of the leak parameter again, since if the CoM bound is very low, the leak will make the decision variable go to zero which would be near the CoM bound, making easier the reversal due to the internal noise.

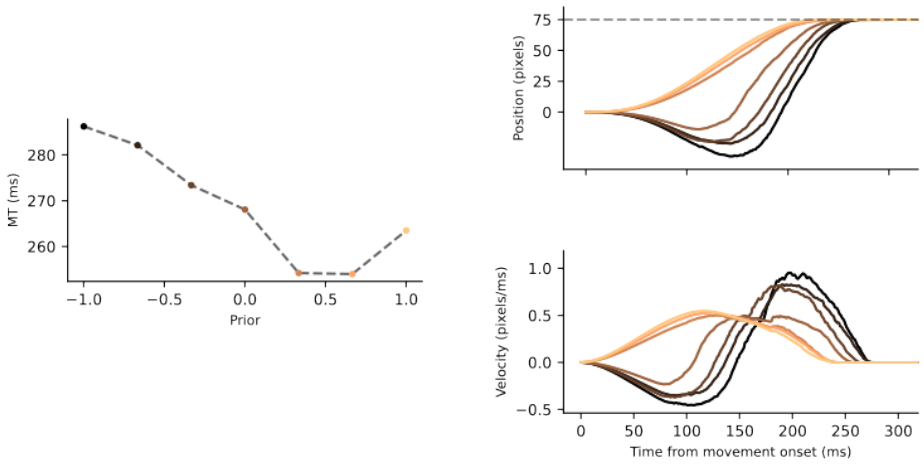

Figure 5.5: MT vs prior evidence (left). Right: Trajectories (top) and velocities (bottom) conditioned to prior evidence. All for silent trials, i.e. no stimulus presented. Simulations of Rat LE42.

The same happens for the stimulus evidence, some individual simulated rats have it fitted very well (Fig. 5.6). Because in express responses the sensory evidence influences the decision variable only at the second read-out (the stimulus information cannot impact the decision variable at the first read-out due to afferent and efferent delays), the impact of the stimulus on the trajectory tends to occur later than that of the prior, as observed in experimental rat data (Fig. 2.7).

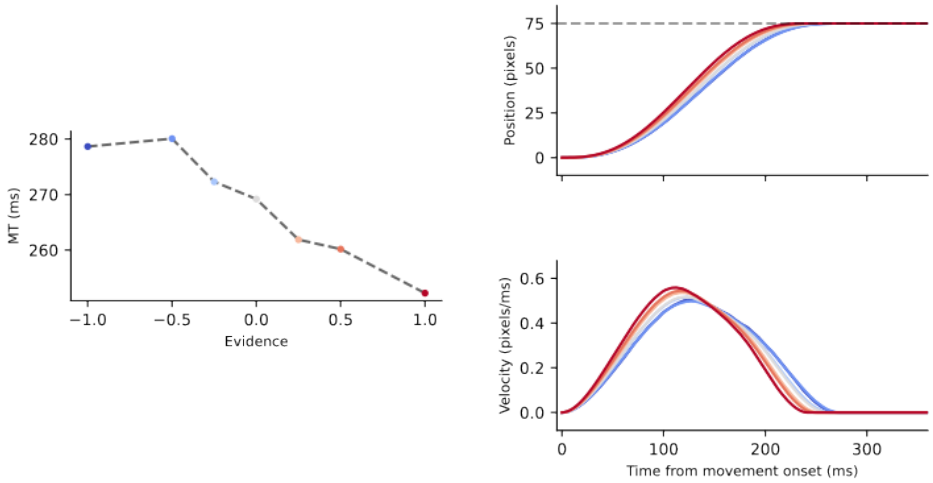

Figure 5.6: MT vs prior evidence (left). Right: Trajectories (top) and velocities (bottom) conditioned to stimulus evidence and RT $<$ 50 ms. Simulations done with a rat without silent trials, LE39.

What we have seen is that the rats for which the model fitted the best the prior dependency, had silent trials ($\sim$ 6.7% of the trials, 6 out of 15 rats); but not fitted at all the stimulus relationship. Whereas rats without silent trials (9 out of 15) fitted very well the stimulus dependency but not the prior. That happens as a consequence of the correlation between the prior and the ground truth, because the prior is an inference of the rat. Hence, when no stimulus is presented, the unique magnitude available to do the choice is the prior evidence, whose weight will be boosted by the optimizer to fit the choice. On the other hand, for rats without silent trials, the optimizer finds the minima to fit the choice only with the stimulus, and do not combine it with the prior. Therefore, since there are more rats without silent trials, the average will show better fits for stimulus but not for prior. Hence, we must focus in the parameters fitted for all rats and understand the combinations of them that give rise to the rats' behavior.

5.1.4 Reversals

Regarding the reversals, the model produces trajectory reversals for changes-of-mind that produce a deflection large enough to be detected by our detection method (Fig. 5.7). These trajectory reversals occur in the same conditions as the animals, reversing their initial trajectory when the stimulus is strongly incongruent with the prior (Fig. 5.8). Interestingly, our model also predicts that only a fraction of the CoMs produces detected trajectory reversals (12% CoMs vs 6% detected reversals): half of the CoMs produced by the model occur before the trajectory has significantly departed from the center line (y=0), and the deflection is too small to be detected.
On the other hand, we see that simulated reversal trajectories for each rat (light salmon in Fig. 5.7) are very heterogeneous. That is because parameters obtained by different rats sometimes differ by orders of magnitude (Appendix C, Fig. C.1), which seems unrealistic, since the behavior of rats is quite stereotyped. This could be solved by restricting the bounds in Θ for the optimizer or imposing some constraints between parameters, so in the end, all parameters (and more importantly, their combinations) fall in a realistic range. This way, we could decrease the leak parameter and the weight of the noise so the prior and stimulus effects would be higher than now.

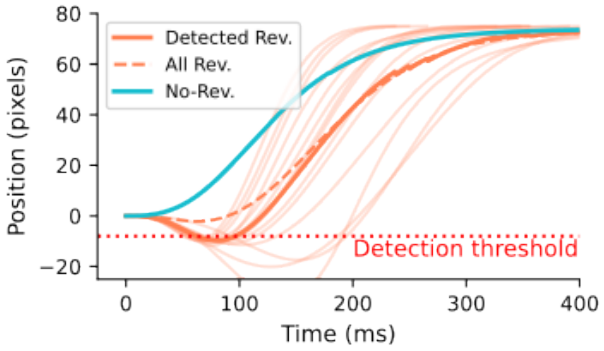

Figure 5.7: Simulated trajectory reversals. Individual subject's simulated reversal trajectories in light salmon.

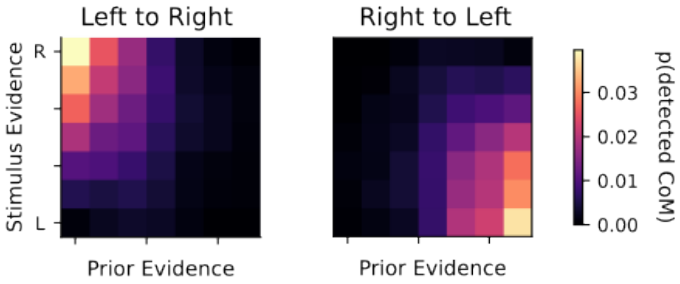

Figure 5.8: Simulated probability of reversal (i.e. detected CoM) matrices.

Even though the average fitting was not perfect, we could still extract some conclusions. So we have seen that our model can explain the behavior of rats, but we need to improve the fitting technique.

6. Conclusions

In this project, I investigated how the accumulation of decision evidence shapes response trajectories in a task where freely-moving rats (and humans) combine prior expectations and acoustic information to select between two possible responses. The main conclusions of the work are the following:

- There is tight and graded relationship between the evidence accumulated during perceptual decisions and the kinematics of the response trajectories described by rats (Section 2) and humans (Section 2.3) to execute their choices.
- Subjects often incorporate the sensory evidence into the trajectory en route, by adjusting its vigor or by changing the planned choice when there is enough evidence contradicting the initial decision (Section 2).
- Rats' trajectories can be approximated by minimizing the jerk of their movement (Section 3.2.5).
- I have encapsulated these results in a computational model that describes both the dynamics of evidence accumulation and the response trajectories, and explains the conditions yielding changes of mind (CoMs) (Section 3).
- To develop the model, I used stochastic differential systems for sensory integration (Section 3.1) and optimal control theory for trajectory generation (Section 3.2).
- The model can capture the impact of the prior and stimulus evidence on choices and response trajectories (Sections 3.6 and 5).
- The model can explain the behavior of both rats (Sections 3.6 and 5) and humans, given that we have found a remarkably similar behavior between them (Section 2.3).
- The model makes several predictions for further experiments:
  - First, it predicts that subjects perform more changes of mind than what is apparent from identifying trajectory reversals (Section 5.1.4). These changes of mind could be detected by "neural reversals", i.e. changes in the sign of the decision variable driven by sensory evidence that that occur before the subject has started moving and that correlate with changes in the stimulus evidence, as observed in rats [23] and monkeys [22, 10, 57].
  - Second, our model shows that just by adding a second readout of the accumulated evidence we can faithfully model the behavior of the subjects (Sections 3.6 and 5). In future experiments, it will be important to test this prediction of the model. One possible way to do it is to design a close-loop paradigm in which the stimulus provided to the subject depends on its current position and velocity, to determine whether animals are able to update their trajectory at any moment during their response trajectory.

6.1 Future work

- We have seen that the model's trajectories differ of the rats' at the beginning, since rats stay at $y = 0$, due to space limitations of the setup, for a short time at the beginning of the trajectory. Hence, I could investigate how to include this in the model so it becomes more realistic.

- Given that the minimum-jerk trajectories do not fully explain the movement of rats, we could explore different combinations of time derivatives of position for minimization (e.g. minimize jerk and acceleration at the same time), to understand how the body moves and which quantities are minimized.
- Improve the fitting method:
  - Train the network with more simulations (I am thinking in the order of 10^7 simulations) so the approximation of the likelihood is more accurate.
  - Changing the optimizer. Extract posterior distributions of the parameters using Markov-Chain Monte Carlo (MCMC) algorithms. I am thinking of using an algorithm developed in the same laboratory that developed BADS [55], which is the Variational Bayesian Monte Carlo (VBMC) [58]. It is an approximate inference method used to fit and evaluate computationally expensive models.
- Fit human data to the model. Once I find the best way to fit the model, fitting the human data (or any other dataset) could be done easily.
- Compare the model with alternative models to evaluate other possible mechanisms that could explain the behavior observed in rats and humans. For example, analyze what happens if we simulate more than two readouts.
- Gather electrohpysiological data to disentangle the brain activity responsible of these decisions and movements.

References

[1] Jason P Gallivan, Craig S Chapman, Daniel M Wolpert, and J Randall Flanagan. Decision-making in sensorimotor control. *Nat. Rev. Neurosci.*, 19(9):519–534, September 2018.

[2] Joshua A Seideman, Terrence R Stanford, and Emilio Salinas. Saccade metrics reflect decision-making dynamics during urgent choices. *Nat. Commun.*, 9(1):2907, July 2018.

[3] Reza Shadmehr and Steven P. Wise. *The Computational Neurobiology of Reaching and Pointing*. The MIT Press, 2005.

[4] Erik M Summerside, Reza Shadmehr, and Alaa A Ahmed. Vigor of reaching movements: reward discounts the cost of effort. *J. Neurophysiol.*, 119(6):2347–2357, June 2018.

[5] Minnan Xu-Wilson, David S Zee, and Reza Shadmehr. The intrinsic value of visual information affects saccade velocities. *Exp. Brain Res.*, 196(4):475–481, July 2009.

[6] David M Milstein and Michael C Dorris. The influence of expected value on saccadic preparation. *J. Neurosci.*, 27(18):4810–4818, May 2007.

[7] Joo-Hyun Song and Ken Nakayama. Hidden cognitive states revealed in choice reaching tasks. *Trends Cogn. Sci.*, 13(8):360–366, August 2009.

[8] Caleb Stone, Jason B Mattingley, and Dragan Rangelov. On second thoughts: changes of mind in decision-making. *Trends Cogn. Sci.*, 26(5):419–431, May 2022.

[9] Roozbeh Kiani, Leah Corthell, and Michael N Shadlen. Choice certainty is informed by both evidence and decision time. *Neuron*, 84(6):1329–1342, December 2014.

[10] Matthew T Kaufman, Mark M Churchland, Stephen I Ryu, and Krishna V Shenoy. Vacillation, indecision and hesitation in moment-by-moment decoding of monkey motor cortex. *Elife*, 4:e04677, May 2015.

[11] Arbora Resulaj, Roozbeh Kiani, Daniel M Wolpert, and Michael N Shadlen. Changes of mind in decision-making. *Nature*, 461(7261):263–266, September 2009.

[12] Ronald van den Berg, Kavitha Anandalingam, Ariel Zylberberg, Roozbeh Kiani, Michael N Shadlen, and Daniel M Wolpert. A common mechanism underlies changes of mind about decisions and confidence. *Elife*, 5:e12192, February 2016.

[13] Ainhoa Hermoso-Mendizabal, Alexandre Hyafil, Pavel E Rueda-Orozco, Santiago Jaramillo, David Robbe, and Jaime de la Rocha. Response outcomes gate the impact of expectations on perceptual decisions. *Nat. Commun.*, 11(1):1057, February 2020.

[14] Laura Busse, Asli Ayaz, Neel T Dhruv, Steffen Katzner, Aman B Saleem, Marieke L Schölvinck, Andrew D Zaharia, and Matteo Carandini. The detection of visual contrast in the behaving mouse. *J. Neurosci.*, 31(31):11351–11361, August 2011.

[15] I Frund, F A Wichmann, and J H Macke. Quantifying the effect of intertrial dependence on perceptual decisions, 2014.

[16] Arman Abrahamyan, Laura Luz Silva, Steven C Dakin, Matteo Carandini, and Justin L Gardner. Adaptable history biases in human perceptual decisions, 2016.

[17] Anke Braun, Anne E Urai, and Tobias H Donner. Adaptive history biases result from Confidence-Weighted accumulation of past choices. *J. Neurosci.*, 38(10):2418–2429, March 2018.

[18] Manuel Molano-Mazón, Yuxiu Shao, Daniel Duque, Guangyu Robert Yang, Srdjan Ostojic, and Jaime de la Rocha. Recurrent networks endowed with structural priors explain suboptimal animal behavior. *Curr. Biol.*, January 2023.

[19] Alexander Mathis, Pranav Mamidanna, Kevin M Cury, Taiga Abe, Venkatesh N Murthy, Mackenzie Weygandt Mathis, and Matthias Bethge. DeepLabCut: markerless pose estimation of user-defined body parts with deep learning. *Nat. Neurosci.*, 21(9):1281–1289, September 2018.

[20] J. Panovska-Griffiths, C.C. Kerr, W. Waites, and R.M. Stuart. Mathematical modeling as a tool for policy decision making: Applications to the COVID-19 pandemic. In *Handbook of Statistics*, pages 291–326. Elsevier, 2021.

[21] Lluís Hernández-Navarro, Ainhoa Hermoso-Mendizabal, Daniel Duque, Jaime de la Rocha, and Alexandre Hyafil. Proactive and reactive accumulation-to-bound processes compete during perceptual decisions. *Nat. Commun.*, 12(1):7148, December 2021.

[22] Roozbeh Kiani, Christopher J Cueva, John B Reppas, and William T Newsome. Dynamics of neural population responses in prefrontal cortex indicate changes of mind on single trials. *Curr. Biol.*, 24(13):1542–1547, July 2014.

[23] J Tyler Boyd-Meredith, Alex T Piet, Emily Jane Dennis, Ahmed El Hady, and Carlos D Brody. Stable choice coding in rat frontal orienting fields across model-predicted changes of mind. *Nat. Commun.*, 13(1):3235, June 2022.

[24] Georg F Striedter and R Glenn Northcutt. *Brains Through Time: A Natural History of Vertebrates*. Oxford University Press, December 2019.

[25] Robert S Turner and Michel Desmurget. Basal ganglia contributions to motor control: a vigorous tutor. *Curr. Opin. Neurobiol.*, 20(6):704–716, December 2010.

[26] Sten Grillner and Brita Robertson. The basal ganglia over 500 million years. *Curr. Biol.*, 26(20):R1088–R1100, October 2016.

[27] Jeremy Gordon, Antonella Maselli, Gian Luca Lancia, Thomas Thiery, Paul Cisek, and Giovanni Pezzulo. The road towards understanding embodied decisions. *Neurosci. Biobehav. Rev.*, 131:722–736, December 2021.

[28] Russell J. Boag, Luke Strickland, Andrew Heathcote, Andrew Neal, Hector Palada, and Shayne Loft. Evidence accumulation modelling in the wild: understanding safety-critical decisions. *Trends in Cognitive Sciences*, 27(2):175–188, feb 2023.

[29] Roger Ratcliff and Gail McKoon. The diffusion decision model: theory and data for two-choice decision tasks. *Neural Comput.*, 20(4):873–922, April 2008.

[30] R Ratcliff. Theoretical interpretations of the speed and accuracy of positive and negative responses. *Psychol. Rev.*, 92(2):212–225, April 1985.

[31] John Palmer, Alexander C Huk, and Michael N Shadlen. The effect of stimulus strength on the speed and accuracy of a perceptual decision. *J. Vis.*, 5(5):376–404, May 2005.

[32] Rafal Bogacz, Eric-Jan Wagenmakers, Birte U Forstmann, and Sander Nieuwenhuis. The neural basis of the speed–accuracy tradeoff. *Trends Neurosci.*, 33(1):10–16, January 2010.

[33] Jose L Pardo-Vazquez, Juan R Castiñeiras-de Saa, Mafalda Valente, Iris Damião, Tiago Costa, M Inês Vicente, André G Mendonça, Zachary F Mainen, and Alfonso Renart. The mechanistic foundation of weber's law. *Nat. Neurosci.*, 22(9):1493–1502, September 2019.

[34] Anne E Urai, Jan Willem de Gee, Konstantinos Tsetsos, and Tobias H Donner. Choice history biases subsequent evidence accumulation. *Elife*, 8, July 2019.

[35] Rafal Bogacz, Eric Brown, Jeff Moehlis, Philip Holmes, and Jonathan D. Cohen. The physics of optimal decision making: A formal analysis of models of performance in two-alternative forced-choice tasks. *Psychological Review*, 113(4):700–765, 2006.

[36] Andrea M. Mitofsky. *Direct Energy Conversion*. CreateSpace Independent Publishing Platform, 2018.

[37] David Morin. *Introduction to Classical Mechanics*. Cambridge University Press, 2008.

[38] L. M. Graves, N. I. Akhiezer, Aline H. Frink, and L. E. Elsgolc. The calculus of variations. *The American Mathematical Monthly*, 71(2):224, feb 1964.

[39] Richard Courant and David Hilbert. *Methods of Mathematical Physics, Vol. 1*. New York: Interscience Publishers, Inc., 1937.

[40] T Flash and N Hogan. The coordination of arm movements: an experimentally confirmed mathematical model. *The Journal of Neuroscience*, 5(7):1688–1703, jul 1985.

[41] E Bizzi, N Accornero, W Chapple, and N Hogan. Posture control and trajectory formation during arm movement. *The Journal of Neuroscience*, 4(11):2738–2744, nov 1984.

[42] N. Hogan. Adaptive control of mechanical impedance by coactivation of antagonist muscles. *IEEE Transactions on Automatic Control*, 29(8):681–690, aug 1984.

[43] Emanuel Todorov and Michael I. Jordan. Smoothness maximization along a predefined path accurately predicts the speed profiles of complex arm movements. *Journal of Neurophysiology*, 80(2):696–714, aug 1998.

[44] Paolo Viviani and Tamar Flash. Minimum-jerk, two-thirds power law, and isochrony: converging approaches to movement planning. *Journal of Experimental Psychology: Human Perception and Performance*, 21(1):32–53, 1995.

[45] Song Lu, Bingxiao Ding, and Yangmin Li. Minimum-jerk trajectory planning pertaining to a translational 3-degree-of-freedom parallel manipulator through piecewise quintic polynomials interpolation. *Advances in Mechanical Engineering*, 12(3):168781402091366, mar 2020.

[46] Mehrdad Yazdani, Geoffrey Gamble, Gavin Henderson, and Robert Hecht-Nielsen. A simple control policy for achieving minimum jerk trajectories. *Neural Networks*, 27:74–80, mar 2012.

[47] Ying-Shi WANG, Lei SUN, Lu ZHOU, and Jing-Tai LIU. Online minimum-acceleration trajectory planning with the kinematic constraints. *Acta Automatica Sinica*, 40(7):1328–1338, jul 2014.

[48] Tzon-Tzer Lu and Sheng-Hua Shiou. Inverses of 2×2 block matrices. *Computers &amp Mathematics with Applications*, 43(1-2):119–129, jan 2002.

[49] R. Thiru Senthil. Blockwise inversion and algorithms for inverting large partitioned matrices, 2023.

[50] Jan Boelts, Jan-Matthis Lueckmann, Richard Gao, and Jakob H Macke. Flexible and efficient simulation-based inference for models of decision-making. *Elife*, 11, July 2022.

[51] Alvaro Tejero-Cantero, Jan Boelts, Michael Deistler, Jan-Matthis Lueckmann, Conor Durkan, Pedro Gonçalves, David Greenberg, and Jakob Macke. sbi: A toolkit for simulation-based inference. *Journal of Open Source Software*, 5(52):2505, aug 2020.

[52] George Papamakarios. Neural density estimation and likelihood-free inference, 2019.

[53] Jan-Matthis Lueckmann, Giacomo Bassetto, Theofanis Karaletsos, and Jakob H. Macke. Likelihood-free inference with emulator networks. 2018.

[54] Qiao Liu, Jiaze Xu, Rui Jiang, and Wing Hung Wong. Density estimation using deep generative neural networks. *Proceedings of the National Academy of Sciences*, 118(15), apr 2021.

[55] Luigi Acerbi and Wei Ji Ma. Practical bayesian optimization for model fitting with bayesian adaptive direct search, 2017.

[56] Charles Audet and J. E. Dennis. Mesh adaptive direct search algorithms for constrained optimization. *SIAM Journal on Optimization*, 17(1):188–217, jan 2006.

[57] Diogo Peixoto, Jessica R Verhein, Roozbeh Kiani, Jonathan C Kao, Paul Nuyujukian, Chandramouli Chandrasekaran, Julian Brown, Sania Fong, Stephen I Ryu, Krishna V Shenoy, and William T Newsome. Decoding and perturbing decision states in real time. *Nature*, 591(7851):604–609, March 2021.

[58] Luigi Acerbi. Variational bayesian monte carlo, 2018.

A. Appendix: Extra Analysis

A.1 Human Behavior

We wondered to what extent the results presented for rats were general across species. I replicated the results obtained in rats in a novel task in human participants (n=20) that mimicked the rat task. Subjects performed an auditory intensity judgment task by moving their finger on a tablet from a fixation point to one of two possible response points (Fig. A.1). As in the rats' task, the probability of repeating the previous correct side varied between Repeating and Alternating blocks, so participants could leverage on the recent trial history to generate prior expectations for the stimulus category. In contrast with the rat's paradigm, we explicitly inserted an urgency component into the task: subjects had to initiate their response within 300 ms after stimulus onset for the trial to be counted as valid.

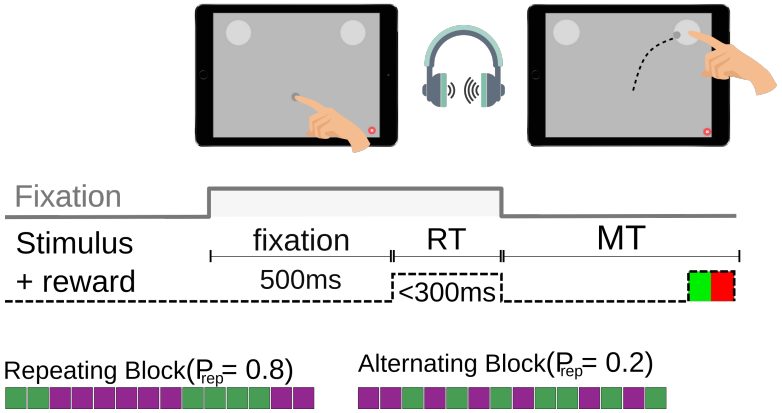

Figure A.1: Human analogous task.

I found a remarkably similar behavior between rats and humans. First, we can see that both sources of information are also exploited (Fig. A.2), as in rats.

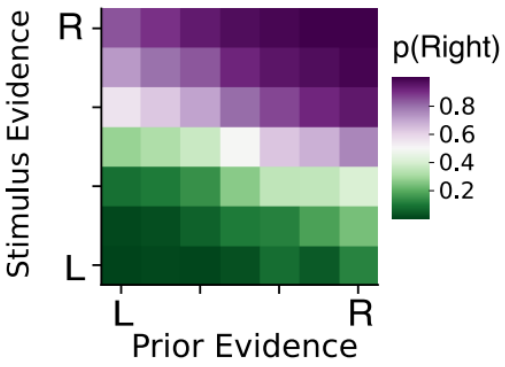

Figure A.2: Human probability of right matrix.

Then, regarding the trajectories, which were extracted using the coordinates of the tablet screen where the finger was placed (Fig. A.3), had a very characteristic shape too.

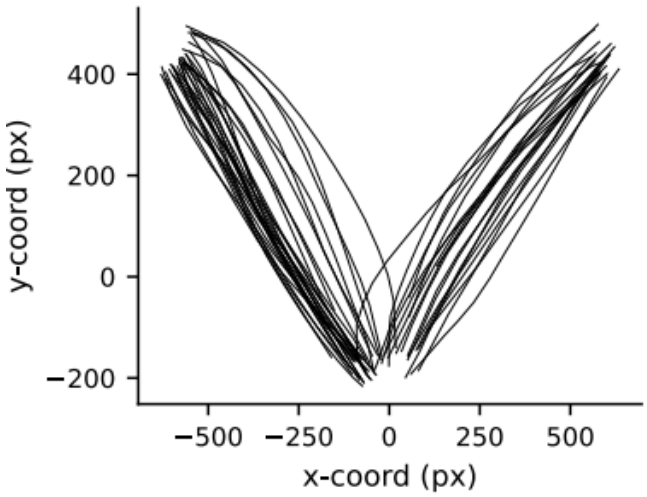

Figure A.3: Human trajectories in the x-y plane.

After conditioning the x-axis trajectory to stimulus and prior evidence, I found that these magnitudes affect the vigor and the trajectory in a similar qualitative way as for rats (Fig. A.4).

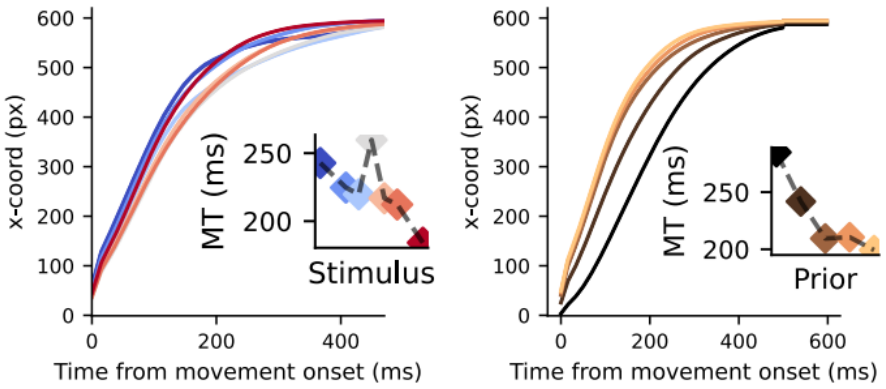

Figure A.4: Human trajectories in the x-axis, conditioned to stimulus evidence (left) and prior evidence (right).

I have also found trajectory reversals in humans, with a very specific shape (Fig. A.5).

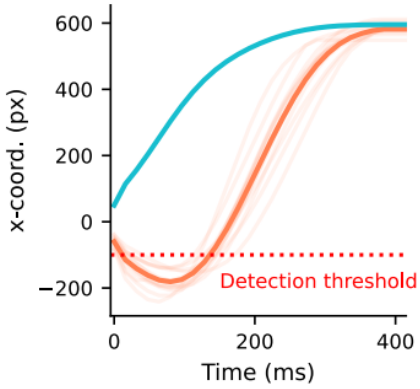

Figure A.5: Human trajectories with average reversal trajectory.

In average, humans tend to do much more reversals than rats. And is the incongruency between prior and stimulus which triggers this phenomena (Fig. A.6).

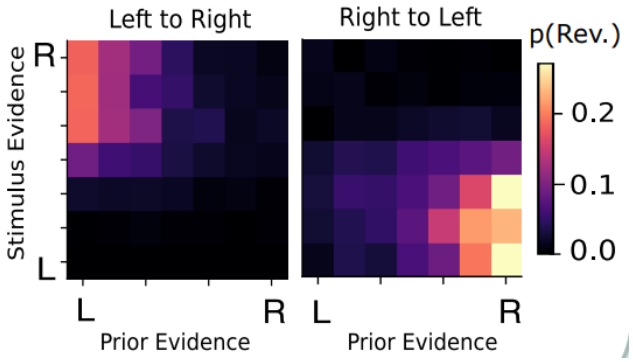

Figure A.6: Probability of reversal matrices for humans.

B. Appendix: Matrix M inversion

In this section, I will present the process of inversion of matrix M to solve (14) of section 3.2.4. The matrix M is

$$M(t_0, t_f) = \begin{pmatrix} 1 & t_0 & t_0^2 & t_0^3 & t_0^4 & t_0^5 \\ 0 & 1 & 2t_0 & 3t_0^2 & 4t_0^3 & 5t_0^4 \\ 0 & 0 & 2 & 6t_0 & 12t_0^2 & 20t_0^3 \\ 1 & t_f & t_f^2 & t_f^3 & t_f^4 & t_f^5 \\ 0 & 1 & 2t_f & 3t_f^2 & 4t_f^3 & 5t_f^4 \\ 0 & 0 & 2 & 6t_f & 12t_f^2 & 20t_f^3 \end{pmatrix} .$$

To start with the inversion process, we express the matrix $M(t_0, t_f)$ as its partitioned version with $3x3$ matrix sub-blocks:

$$M(t_0, t_f) = \begin{pmatrix} \mathbf{A} & \mathbf{B} \\ \mathbf{C} & \mathbf{D} \end{pmatrix} \text{ with } \mathbf{A} = \begin{pmatrix} 1 & t_0 & t_0^2 \\ 0 & 1 & 2t_0^2 \\ 0 & 0 & 2 \end{pmatrix} , \mathbf{B} = \begin{pmatrix} t_0^3 & t_0^4 & t_0^5 \\ 3t_0^2 & 4t_0^3 & 5t_0^4 \\ 6t_0 & 12t_0^2 & 20t_0^3 \end{pmatrix}$$

and analogously for $\mathbf{C}$ and $\mathbf{D}$ with t_e instead of t_0. Then, we can express the inverse as a solution of

$$M\, M^{-1} = \begin{pmatrix} \mathbf{A} & \mathbf{B} \\ \mathbf{C} & \mathbf{D} \end{pmatrix} \begin{pmatrix} \mathbf{W} & \mathbf{X} \\ \mathbf{Y} & \mathbf{Z} \end{pmatrix} = \begin{pmatrix} \mathbf{I} & 0 \\ 0 & \mathbf{I} \end{pmatrix} ,$$

then, on one side, we have

$$\mathbf{AX} + \mathbf{BZ} = 0 \rightarrow \mathbf{X} = -\mathbf{A}^{-1}\mathbf{BZ} .$$

Since $\mathbf{A}$ is upper-triangular and the diagonal entries are non-zero, it is non-singular (i.e. can be inverted). On the other side, we have that

$$\mathbf{CX} + \mathbf{DZ} = \mathbf{I} \rightarrow \mathbf{Z} = (\mathbf{D} - \mathbf{CA}^{-1}\mathbf{B})^{-1} .$$

We assume that $(\mathbf{D} - \mathbf{CA}^{-1}\mathbf{B})^{-1}$ is invertible. Continuing with the computation, we use now that the inverse, by definition, satisfies

$$M\, M^{-1} = M^{-1}\, M = \mathbf{I}.$$

This way, we can express $\mathbf{W}$ and $\mathbf{Y}$ in terms of $\mathbf{X}$ and $\mathbf{Z}$, which are known. Then, we have that

$$\mathbf{YA} + \mathbf{ZC} = 0 \rightarrow \mathbf{Y} = -\mathbf{ZCA}^{-1} ,$$

with $\mathbf{Z}$ known. Finally, we have that

$$\mathbf{WA} + \mathbf{XC} = \mathbf{I} \rightarrow \mathbf{W} = \mathbf{A}^{-1} - \mathbf{XCA}^{-1} ,$$

with $\mathbf{X}$ known. Then, the final expression for the inverse of M, M^{-1} is

$$M(t_0, t_f)^{-1} = \begin{pmatrix} \mathbf{W} & \mathbf{X} \\ \mathbf{Y} & \mathbf{Z} \end{pmatrix} = \begin{pmatrix} \mathbf{A}^{-1} + \mathbf{A}^{-1}\mathbf{B}(\mathbf{D} - \mathbf{CA}^{-1}\mathbf{B})^{-1}\mathbf{CA}^{-1} & -\mathbf{A}^{-1}\mathbf{B}(\mathbf{D} - \mathbf{CA}^{-1}\mathbf{B})^{-1} \\ -(\mathbf{D} - \mathbf{CA}^{-1}\mathbf{B})^{-1}\mathbf{CA}^{-1} & (\mathbf{D} - \mathbf{CA}^{-1}\mathbf{B})^{-1} \end{pmatrix} .$$

In order to simplify the expression, if $t_0 = 0$, the matrix $\mathbf{B}$ becomes a $3x3$ zero matrix and $\mathbf{A}$ a pure diagonal matrix, which inverse is easy to compute. Then, the expression of the inverse of M becomes much simpler

$$M(t_0 = 0, t_f)^{-1} = \begin{pmatrix} \mathbf{A}^{-1} & \mathbf{0} \\ -\mathbf{D}^{-1}\mathbf{CA}^{-1} & \mathbf{D}^{-1} \end{pmatrix}$$

which the only components that must be inverted are $\mathbf{A}$ and $\mathbf{D}$. Since now $\mathbf{A}$ is diagonal, its inverse is just the inverse of each entry in the diagonal

$$\mathbf{A}^{-1} = \begin{pmatrix} 1 & 0 & 0 \\ 0 & 1 & 0 \\ 0 & 0 & 1/2 \end{pmatrix}$$

and for the inverse of $\mathbf{D}$, we first must show that it is non-singular, so we compute its determinant

$$\det \mathbf{D} = t_f^{-9}/2 \,,$$

which tends to zero when $t_f \to \infty$, which is unrealistic. Therefore the matrix is non-singular for realistic values of t_f. We can compute the inverse as

$$\mathbf{D}^{-1} = \frac{\text{adj}(\mathbf{D})}{\det(\mathbf{D})} = \begin{pmatrix} 10/t_f^3 & -4/t_f^2 & 1/2t_f \\ -15/t_f^4 & 7/t_f^3 & -1/t_f^2 \\ 6/t_f^5 & -3/t_f^4 & 1/2t_f^3 \end{pmatrix}$$

where adj$(\cdot)$ is the adjugate and det$(\cdot)$ the determinant. Then, after basic computations, the inverse of M terms of t_f becomes

$$M(t_0 = 0, t_f)^{-1} = \begin{pmatrix} 1 & 0 & 0 & 0 & 0 & 0 \\ 0 & 1 & 0 & 0 & 0 & 0 \\ 0 & 0 & 1/2 & 0 & 0 & 0 \\ -10/t_f^3 & -6/t_f^2 & -3/2t_f & 10/t_f^3 & -4/t_f^2 & 1/2t_f \\ 15/t_f^4 & 8/t_f^3 & 3/2t_f^2 & -15/t_f^4 & 7/t_f^3 & -1/t_f^2 \\ -6/t_f^5 & -3/t_f^4 & -1/2t_f^3 & 6/t_f^5 & -3/t_f^4 & 1/2t_f^3 \end{pmatrix}$$

and in our case, we have that the final time t_f is the Movement Time (MT), $t_f = MT$.

C. Appendix: Model fitting

In this section, we will take a look at the results of the fitting, i.e. the parameters extracted for each rat. We can take a look at the distributions of fitted parameters (Fig. C.1), to see that there are some (mainly related to time delays) which the optimizer found the minima of the likelihood in the bounds. Meaning that I should train the network with larger initialization space and run the optimizer with less restrictive bounds and see where does it find this minima. Moreover, leak is also in its maximum, in our model then rats forget 70% of the information.

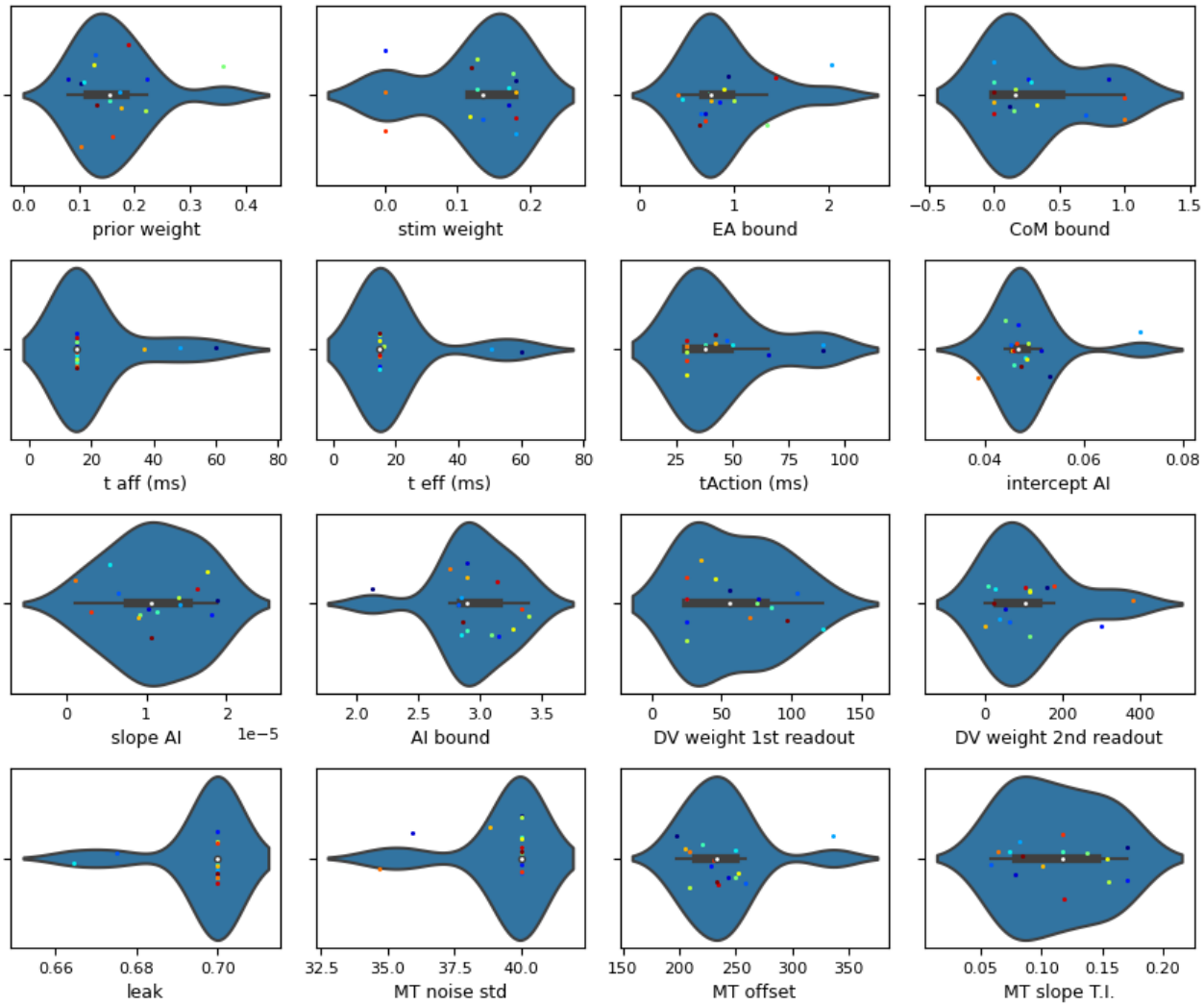

Figure C.1: Fitted parameters distributions for all rats.